

# Osteology and relationships of *Olorotitan arharensis*, a hollow-crested hadrosaurid dinosaur from the latest Cretaceous of Far Eastern Russia

PASCAL GODEFROIT, YURI L. BOLOTSKY, and IVAN Y. BOLOTSKY



Godefroit, P., Bolotsky, Y.L., and Bolotsky, I.Y. 2012. Osteology and relationships of *Olorotitan arharensis*, a hollow-crested hadrosaurid dinosaur from the latest Cretaceous of Far Eastern Russia. *Acta Palaeontologica Polonica* 57 (3): 527–560.

The holotype of *Olorotitan arharensis* from the Maastrichtian Udurchukan Formation in Kundur, Far Eastern Russia, is the most complete dinosaur discovered in Russia and one of the best preserved lambeosaurines outside western North America. This taxon is diagnosed by following autapomorphies: large helmet-like hollow crest higher than the rest of the skull and extending caudally well beyond the level of the occiput; very high postorbital process of jugal (ratio height of postorbital process/length of jugal = 1); rostral portion of the jugal shorter than in other lambeosaurines, with a perfectly straight rostral margin; very asymmetrical maxilla in lateral view, with ventral margin distinctly downturned; very elongated neck composed of 18 cervical vertebrae; tibia as high as the femur; shorter cnemial crest, about one fifth of tibia length. A phylogenetic analysis, based on 118 cranial, dental, and postcranial characters, indicates that *Olorotitan* is a member of the Corythosaurini clade, and is the sister taxon of *Corythosaurus casuarius*, *Hypacrosaurus stebingeri*, and *Hypacrosaurus altispinus*. The high diversity and mosaic distribution of Maastrichtian hadrosaurid faunas in the Amur-Heilongjiang region are the result of a complex palaeogeographical history and imply that many independent hadrosaurid lineages dispersed readily between western America and eastern Asia at the end of the Cretaceous.

Key words: Dinosauria, Ornithischia, Hadrosauridae, Lambeosaurinae, *Olorotitan arharensis*, osteology, phylogeny, Late Cretaceous, Russia.

Pascal Godefroit [Pascal.Godefroit@naturalsciences.be], Royal Belgian Institute of Natural Sciences, rue Vautier 29, 1000 Brussels, Belgium;

Yuri L. Bolotsky [dinomus@ascnet.ru], Palaeontological Laboratory of the Institute of Geology and Nature Management, Far East Branch, Russian Academy of Sciences, per. Relochny 1, 675000 Blagoveschensk, Russia;

Ivan Y. Bolotsky [vargulfr@mail.ru], Palaeontological Laboratory of the Institute of Geology and Nature Management, Far East Branch, Russian Academy of Sciences, per. Relochny 1, 675000 Blagoveschensk, Russia and Research Center for Paleontology and Stratigraphy, Jilin University, Changchun 130061, P.R. China.

Received 13 May 2011, accepted 23 August 2011, available online 9 September 2011.

## Introduction

Four rich dinosaur localities have been discovered in the Amur-Heilongjiang region of eastern Asia (Fig. 1): Jiayin (Riabinin 1930; Godefroit et al. 2001) and Wulaga (Godefroit et al. 2008) in the Yuliangze Formation of northern Heilongjiang Province (China), Blagoveschensk (Bolotsky and Kurzanov 1991; Godefroit et al. 2004b) and Kundur (Godefroit et al. 2003; Van Itterbeeck et al. 2005), in the Udurchukan Formation of southern Amur region (Russia). All these sites are located in south-eastern part (“Lower Zeya depression”) of the Zeya-Bureya sedimentary basin, near its borders with the adjacent uplifted areas, the Lesser Khingang Mountains and the Turan uplift. In these four sites, dinosaur bones form large bonebeds extending over several hundred square metres. In each locality, the dinosaur fauna is largely dominated by lambeosaurine hadrosaurids (Godefroit et al.

2000, 2003, 2004b), but hadrosaurine (non-crested or solid-crested) hadrosaurids are also represented (Bolotsky and Godefroit 2004; Godefroit et al. 2008).

The Kundur locality was discovered in 1990 by Vladimir A. Nagornyi (Far Eastern Institute of Mineral Resources, FEB RAS, Blagoveschensk, Russia), who collected fossil bones in a road section along the Chita-Khabarovsk highway near the village of Kundur. He immediately sent his discoveries to Institute of Geology and Research Exploration of FEB RAS. Large-scale excavations started at Kundur in 1999.

The age of the Kundur locality is subject to debate. Although the three sites belong to the same *Wodehouseia spinata*–*Aquilapollenites subtilis* Palynozone, Markevich and Bugdaeva (2001) dated the Kundur and Jiayin dinosaur localities as early Maastrichtian, whereas Blagoveschensk was dated as “middle” Maastrichtian. The proposed ages

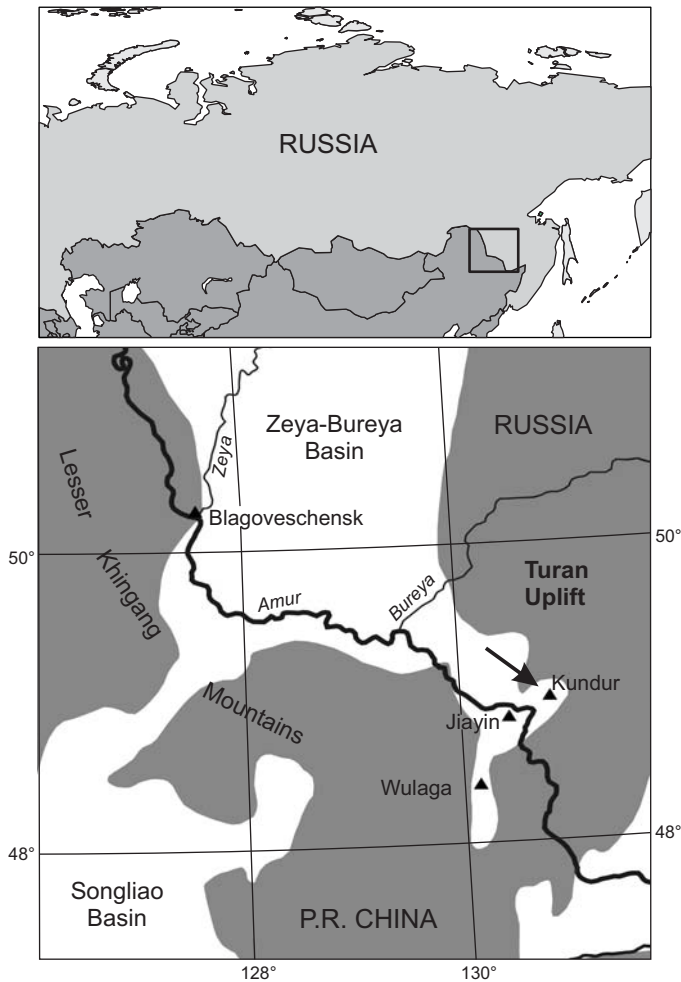


Fig. 1. Map of the Amur-Heilongjiang region indicating the main dinosaur sites (black triangles) discussed in this paper. The Kundur locality is indicated by an arrow. The dark grey zones in the lower diagram indicate the uplifted areas.

were based on comparisons with other palynological assemblages in neighbouring basins (Markevich 1994). Bugdaeva and Markevich (2001) asserted that both the vegetation change and dinosaur extinction in the Russian Far East took place at the locally defined “middle”–upper Maastrichtian boundary. However, Godefroit et al. (2003, 2004b), Van Itterbeeck et al. (2005), and Nichols and Johnson (2008) noted that the pollen assemblage described by Markevich and Bugdaeva (2001) from the Kundur locality resembles the *Wodehouseia spinata* Assemblage Zone of the United States, which is late Maastrichtian in age (Nichols and Sweet 1993; Nichols 2002). Consequently, they proposed that the Udurchukan and Yuliangze Formations are late Maastrichtian in age, not early or “middle” Maastrichtian and that the observed dinosaur extinction and vegetation changes mark the upper Maastrichtian–Paleocene boundary, not the “middle” Maastrichtian–upper Maastrichtian boundary, as proposed earlier. To close this debate, independent indicators (palaeontological, geochronological, or magnetostratigraphic) are yet to be found in the Maastrichtian deposits of the Amur-Heilongjiang region.

The Kundur fauna is not particularly diversified, including lindholmemydid turtle fragments, (Danilov et al. 2002), crocodile teeth, and isolated bones and teeth belonging to theropod (Alifanov and Bolotsky 2002) and nodosaurid (Tumanova et al. 2004) dinosaurs. The first multituberculate mammal fossil from Russia was also described from the Kundur locality (Averianov et al. 2002). Alifanov and Bolotsky (2010) described a new sauropod dinosaur, *Arkharavia heterocoelica*, from caudal vertebrae discovered at Kundur, but those vertebrae likely belong to hadrosaurid dinosaurs. Hadrosaurids are the dominant vertebrates at the Kundur localities. They are represented by the flat-headed saurolophine *Kundurosaurus nagornyi* Godefroit, Bolotsky, and Lauters, 2012, and by the lambeosaurine *Olorotitan arharensis* Godefroit, Bolotsky, and Alifanov, 2003.

The holotype of *Olorotitan arharensis* is an incomplete skeleton discovered in 1999 and completely excavated in 2001. It is the most complete dinosaur skeleton ever discovered in Russia and the most complete lambeosaurine outside North America. Smaller and more fragmentary skeletons that may be referred to as *O. arharensis* were also discovered at Kundur, together with disarticulated bones.

In this paper we describe the skull and skeleton of the holotype of *Olorotitan arharensis* and we discuss its phylogenetic affinities among lambeosaurine dinosaurs.

*Institutional abbreviations.*—AEHM, Amur Natural History Museum of the Far Eastern Institute of Mineral Resources, FEB RAS, Blagoveschensk, Russia; AMNH, American Museum of Natural History, New York, USA; CMN, Canadian Museum of Nature, Ottawa, Canada; GMH, Geological Museum of Heilongjiang, Harbin, China; IVPP, Institute of Vertebrate Paleontology and Paleoanthropology, Beijing, China; PIN, Paleontological Institute of the Russian Academy of Sciences, Moscow, Russia; ROM, Royal Ontario Museum, Toronto, Canada.

*Other abbreviation.*—cn, cranial nerve.

## Taphonomic observations

The sedimentology of the Kundur locality has already been described in detail by Bugdaeva et al. (2001) and Van Itterbeeck et al. (2005). The bonebed covers a surface of at least 1000 m<sup>2</sup>, but the thickness of the fossiliferous horizon does not exceed 1.5 m. The fossil-bearing sediments consist of an olive-grey muddy matrix, with scattered very coarse sand particles and pebbles <2 cm, and can be described as a clast-poor diamict. The clays are dominantly smectite with some illite and kaolinite. The observed mixture of fine and coarse material is typical for gravity flow deposits. The sediments have the characteristics of both debris flows and hyperconcentrated flows (Van Itterbeeck et al. 2005). Only areas with a distinct relief can generate debris flows. Uplifted areas, located at a distance of a few tens of kilometres from the Kundur site, are known along the borders of the Lower

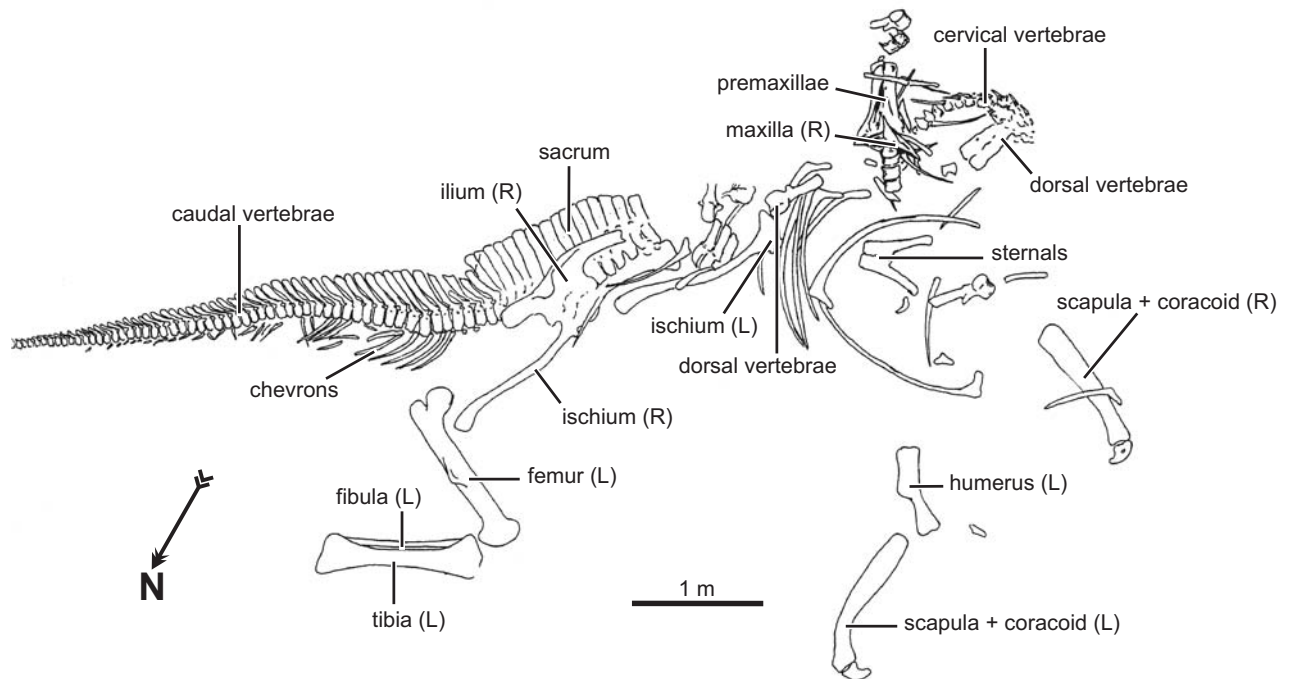


Fig. 2. Holotype (AEHM 2/845) of hadrosaurid dinosaur *Olorotitan arharensis* Godefroit, Bolotsky, and Alifanov, 2003, from the Upper Cretaceous of Kundur (Russia), as discovered in the field (N49°04'57.5", E130°51'34.1"). Abbreviations: L, left; N, North; R, right.

Zeya Depression. Both the Turpan Uplift and the Lesser Khingang mountains are possible source regions for such debris flows, and Markevich and Bugdaeva (2001) favoured the former. This hypothesis is supported by the position of the Kundur site within the basin (see Fig. 1). The large distance between the postulated source region and the Kundur site makes the recorded sediment gravity flow deposits exceptional phenomena, if they are indeed debris flows. However, the dominance of diamicts within the Udurchukan Formation indicates that these sediment gravity flows occurred frequently, and a closer source region cannot be excluded. More detailed palaeogeographical studies are required to determine the true source region, but the lack of exposures in the present-day landscape will make this difficult.

The bonebed consists of a mixture of partially articulated skeletons, together with isolated bones belonging to numerous individuals of different sizes. Most fossils lay in horizontal position but rare vertically oriented bones were also observed. The articulated elements and the long bones have a preferential EW orientation (Van Itterbeeck et al. 2005: fig. 6c), indicating that the bones and carcasses were transported. Voorhies (1969) noticed the tendency of linear elements to align parallel to flow direction if the elements are submerged, but perpendicular if partially emergent.

AEHM 2/845 was discovered lying on its left flank, with its skull, axial skeleton, and pectoral girdle mostly complete and articulated, whereas its limbs were more disarticulated and incomplete. Hands and feet are completely missing (Fig. 2). Some bones (e.g., nasal, quadrates, ischia, ribs) are broken and incomplete. The skull was only slightly disarticulated, but the bones were not displaced far from their original

positions. The lighter and most fragile elements of the skull (e.g., lacrimal, quadratojugal, vomer, palatine, angular, splenial) are not preserved. Perthotaxic features (bone modification processes active on the land surface; see Clark et al. 1967) could not be observed on the bone surface of AEHM 2/845, indicating that the skeleton was not exposed sub-aerially for any significant time. The articulation of most of the skeleton and the absence of perthotaxic features indicates rapid and in situ burial before complete decomposition of the soft parts, within a few days after death (Koster 1987). The horizontal orientation of the skeleton and its uniform preservation indicates that it was buried by one event. A sediment gravity flow can account for the rapid burial of such a large animal and even for its death (Loope et al. 1998, 1999). However, the absence of parts of the skeleton and the disarticulation of the limb bones suggest that it was already partially decomposed before transportation.

The frontal and parietal of AEHM 2/845 are dislocated and the left frontal is pierced by a quadrangular hole (Figs. 4C, 5C). Its outline and size might correspond to the large theropod ("tyrannosaurid") shed teeth that were found in the same layer as this skeleton (Alifanov and Bolotsky 2002). Moreover, several parallel grooves on the right side of the skull around the foramen for cn IV may tentatively be identified as theropod tooth marks (Fiorillo 1988, 1991a, b). It may therefore be hypothesized that AEHM 2/845 was killed by a theropod dinosaur or partly eaten by predators or scavengers before burial. This hypothesis is also consistent with the absence or complete disarticulation of limb elements. However, we could not recognize evident carnivorous tooth marks on the surfaces of the remaining long bones. It may also be hypothesized that

prey were particularly numerous and that scavengers only ate the fleshy parts of carcasses (Eberth and Getty 2005). Fiorillo (1991b) observed that tooth-marked bones are never frequent in dinosaur localities and that theropod dinosaurs did not routinely chew bones during feeding. They may have utilized prey bones in a manner more like modern Komodo monitors and crocodiles than mammalian carnivores; that is, by passive consumption rather than by actively seeking out the bones for nutrient intake.

## Systematic palaeontology

Dinosauria Owen, 1842

Ornithischia Seeley, 1887

Hadrosauridae Cope, 1869

Lambeosaurinae Parks, 1923

Genus *Olorotitan* Godefroit, Bolotsky, and Alifanov, 2003

*Type species*: *Olorotitan arharensis* Godefroit, Bolotsky, and Alifanov, 2003; see below.

*Diagnosis*.—As for type and only species (see below).

*Olorotitan arharensis* Godefroit, Bolotsky, and Alifanov, 2003

Figs. 2–22.

*Holotype*: AEHM 2/845, an articulated, but incomplete adult skeleton including the skull and most of the postcranium, with the exception of several dorsal vertebrae, ribs, proximal haemaphyses, right humerus, right manus, left antebrachium, pubes, right hindlimb, and left pes.

*Type locality*: Kundur (N 49°04'57.5", E 130°51'34.1"), Amur region, Far Eastern Russia.

*Type horizon*: Udurchukan Formation (*Wodehouseia spinata*–*Aquila-pollenites subtilis* Palynozone), ?late Maastrichtian, Late Cretaceous.

*Emended diagnosis*.—Lambeosaurine dinosaur characterized by the following autapomorphies: large helmet-like hollow crest higher than the rest of the skull and extending caudally well beyond the level of the occiput; very high postorbital process of jugal (ratio height of postorbital process/length of jugal = 1); rostral portion of the jugal shorter than in other lambeosaurines, with a perfectly straight rostral margin; asymmetrical maxilla in lateral view, with ventral margin distinctly downturned; elongated neck composed of 18 cervical vertebrae; tibia as long as the femur; short cnemial crest, about one fifth of tibia length.

## Description

### Skull and mandible

Although most of the skull bones were slightly displaced and the nasal is incompletely preserved, the skull of AEHM 2/845 can be accurately reconstructed (Fig. 3). The large crest dominates the skull. In lateral view, the profile of the skull appears slightly concave, and the crest is much higher

than the rest of the skull. It is even higher than in *Lambeosaurus magnicristatus* CMN 8705. The nasal formed most of the caudal part of the crest and likely extended well beyond the level of the occiput. The morphology of the internal nasal passage remains unknown because of the fragmentary nasal and the dorsoventrally crushed premaxillae. All the measurements taken on AEHM 2/845 are compiled in Appendix 1.

*Fused exoccipital-opisthotic*.—Above the foramen magnum, the dorsal side of the exoccipital-opisthotic is more depressed than in *Amurosaurus riabinini* and *Sahaliyana elunchunorum*. The exoccipital condyloids are particularly massive and form the prominent dorsolateral portions of the occipital condyle (Fig. 4E). Caudal to the metotic strut, the lateral side of the occipital condyle is pierced by three foramina for cranial nerves (Figs. 4A, B, 5D). The most caudal foramen is the largest and provided passage for the hypoglossal nerve (cn XII). The vagus canal (for cn X) is set more dorsally and opens medially into the metotic (“jugular”) foramen. According to Evans (2010), the smaller foramen between the vagus and hypoglossal foramina conducted a separate branch of the hypoglossal nerve and not cn XI (contra Godefroit et al. 2004a, b). A horizontal sulcus along the prominent metotic strut (Figs. 4A, 5D) is, according to Ostrom (1961), interpreted as a stapedial recess. Cranial to the metotic strut, a large auditory foramen (Figs. 4A, B, 5D) is divided by an oblique crista interfenestralis into a rostral fenestra ovalis (stapedial recess) and a caudal metotic foramen. The metotic foramen contains separate openings for cn IX (dorsal) and the internal jugular vein (ventral).

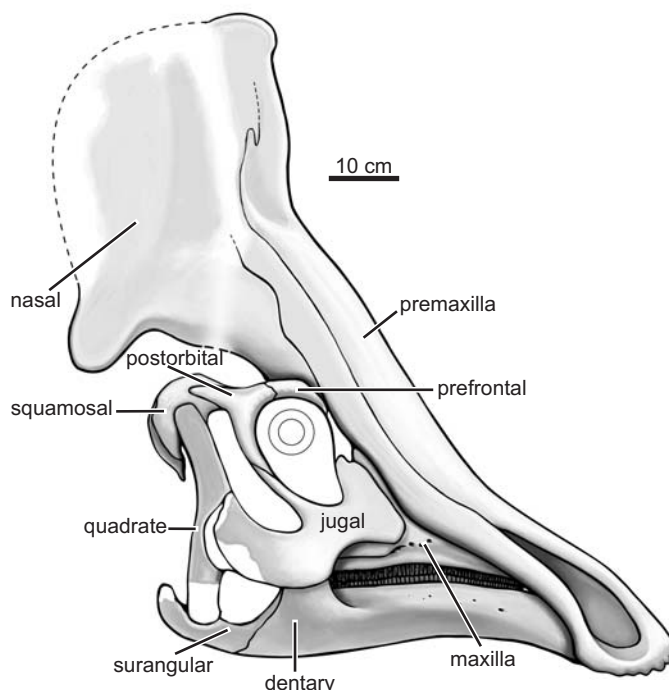


Fig. 3. Reconstruction of the skull of hadrosaurid dinosaur *Olorotitan arharensis* Godefroit, Bolotsky, and Alifanov, 2003, from the Upper Cretaceous of Kundur (Russia), in right lateral view.

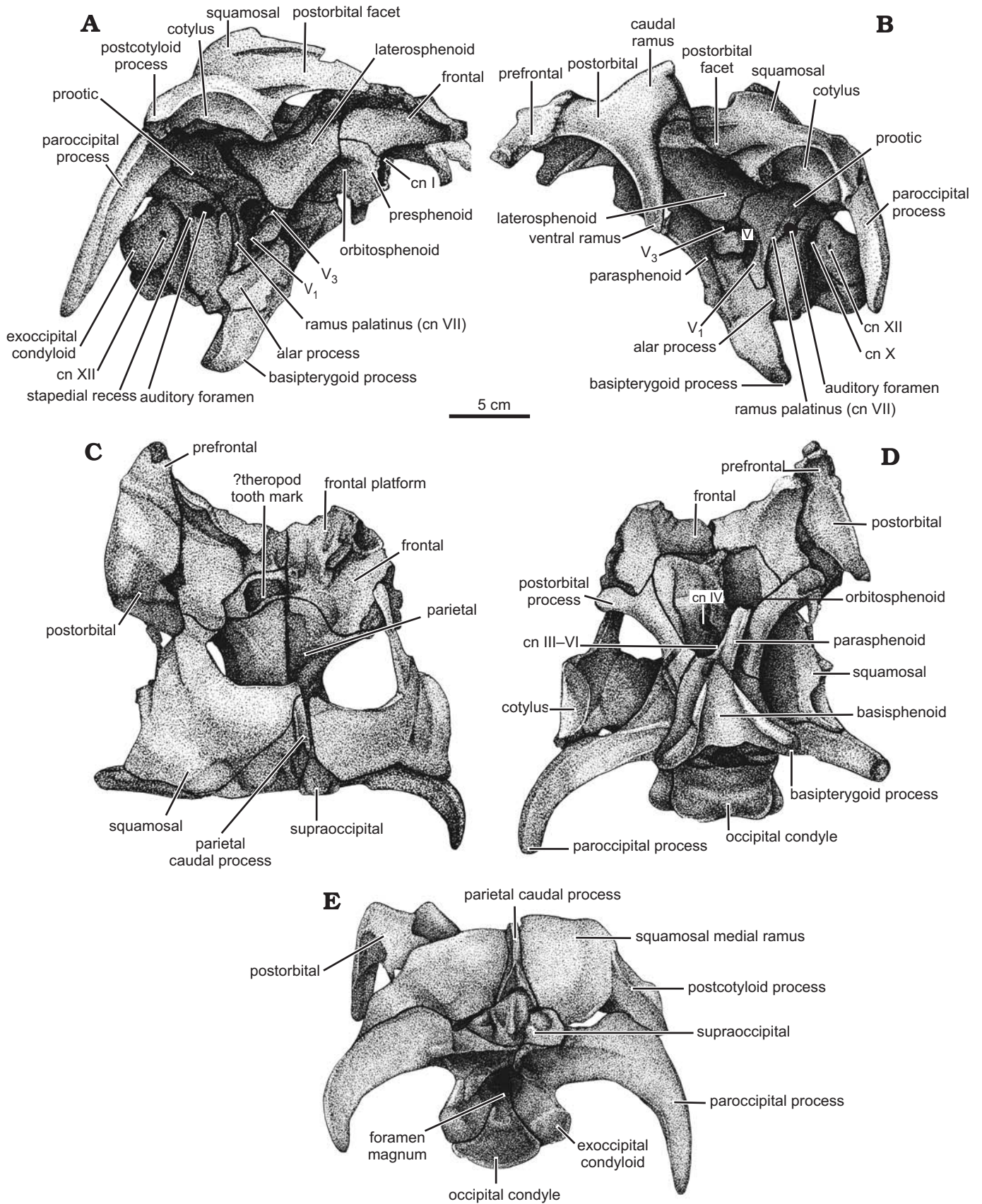


Fig. 4. Interpretative drawings of the braincase of hadrosaurid dinosaur *Olorotitan arharensis* Godefroit, Bolotsky, and Alifanov, 2003 (AEHM 2/845, holotype), from the Upper Cretaceous of Kundur (Russia), in right lateral (A), left lateral (B), dorsal (C), ventral (D), and caudal (E) views. Abbreviation: cn, foramina for cranial nerves.

The paroccipital processes have a pendent aspect and their tip reaches the level of the base of the occipital condyle (Fig. 4E). They are more gracile than in *Amurosauros riabinini*, but more robust than in *Sahaliyana elunchunorum*. As previously described in *Amurosauros riabinini*, the dorsolateral angle of the paroccipital process inserts into a ventral depression of the squamosal in a synovial joint (Fig. 4E).

*Prootic*.—The stout caudodorsal branch of the prootic extensively covers the rostral surface of the paroccipital process and contacts the supraoccipital and the parietal for a short distance. A well-developed crista otosphenoidale extends into the paroccipital process (Fig. 5D). More ventrally, the prootic is notched both by the rostral margin of the auditory recess and by the caudal margin of the large foramen for the Gasserian ganglion of the trigeminal nerve (cn V). From the latter aperture, ramus mandibularis of the trigeminal nerve ( $V_3$ ) forms a ventrally-directed sulcus along the lateral surface of the prootic, just behind the basisphenoid process of the laterosphenoid (Figs. 4A, B, 5D). Between the notches for the auditory foramen and the trigeminal nerve, the lateral side of the prootic bears a narrow and elongated sulcus that housed ramus palatinus of the facial nerve (cn VII; Figs. 4A, B, 5D). The prootic forms a ventral flange that covers the lateral surface of the basisphenoid. The caudoventral ridge that conceals the dorsal part of the carotid canal, in continuity with the alar process of the basisphenoid, is much less developed than in *Amurosauros riabinini*.

*Laterosphenoid*.—The caudal prootic process of the laterosphenoid covers the rostral portion of the prootic. The ventral basisphenoid process (Fig. 5D) forms a prominent foot that covers the alar process of the basisphenoid and the ventral flange of the prootic. The angle between the prootic and basisphenoid processes forms the rostral margin of the trigeminal nerve. The ramus ophthalmicus of the trigeminal nerve ( $V_1$ ) has a wide and deep horizontal sulcus on the basisphenoid process of the laterosphenoid. The rostral margin of the basisphenoid process is notched by the large common foramen for oculomotor (III) and abducens (VI) nerves. The postorbital process of the laterosphenoid extends rostro-laterally to form a synovial articulation with the postorbital (Fig. 4D). The rostral side of the postorbital process articulates with the frontal and the orbitosphenoid.

*Orbitosphenoid*.—The rostroventral part of the braincase is crushed and, consequently, the orbitosphenoid cannot be adequately described. The foramen for the trochlear nerve (IV) is large and located not far from the junction between the orbitosphenoid and the parasphenoid (Fig. 4D).

*Presphenoid*.—The paired presphenoids form the rostral margin of the large median opening for the olfactory nerve (cn I; Fig. 4A) on the rostroventral part of the braincase. Their caudal limit with the orbitosphenoid cannot be discerned. Dorsally, they contact the frontal.

*Basioccipital*.—The basioccipital of *Olorotitan arharensis* is proportionally shortened, about twice as broad as long (Fig. 4D), whereas it is as long as broad in *Amurosauros*. In caudal

view, the occipital condyle is kidney-shaped, low, and incised by a vertical furrow. Its articular surface is perfectly vertical. The dorsomedian side of the basioccipital forms the floor of the foramen magnum (Fig. 4E). There is no distinct neck separating the occipital condyle from the sphenoccipital tubercles. An oblique crest extends along the lateral side of the sphenoccipital tubercles, in continuity with the ventral border of the paroccipital process. In front of this crest, the dorsal side of the basioccipital participates in the ventral border of the auditory foramen.

*Basisphenoid*.—The basisphenoid of *Olorotitan arharensis* is incompletely preserved. The basipterygoid processes extend caudoventrally (Fig. 4A, B), as usual in hadrosaurids (Godefroit et al. 1998). The alar process is eroded, but appears less developed than in *Amurosauros riabinini*.

*Parasphenoid*.—This bone is completely fused to the basisphenoid, so that its limits cannot be discerned. It projects upwardly and forwardly between the orbits. Caudodorsally, it contacts the orbitosphenoid. Caudally, the parasphenoid forms the ventral margin of the common opening for the oculomotor (III) and abducens (VI) nerves (Fig. 4D).

*Supraoccipital*.—The supraoccipital of *Olorotitan arharensis* (Fig. 4E) is identical to that of *Amurosauros riabinini*. Therefore, we refer to Godefroit et al. (2004b) for a detailed description of this bone.

*Parietal*.—Because of the dorsoventral crushing of the braincase, the parietal of AEMH 2/845 is broken in two along its midline (Figs. 4C, 5C). As usual in lambeosaurines, the parietal is shortened: the ratio “length/minimal width”  $< 2$ , and the width of its proximal end equals the length of the bone. As in *Amurosauros riabinini* (AEHM 1/252), *Corythosaurus casuarius* (AMNH 5433), and *Lambeosaurus lambei* (Evans 2010), the parietal length is over 50% the interorbital width of the skull. The parietal is proportionally shorter, being less than 40% of the interorbital width, in *Hypacrosaurus altispinus*, *Hypacrosaurus stebingeri*, *Parasaurolophus walkeri* (Evans 2010), and *Charonosaurus jiayinensis* (PG, personal observation). Rostrally, the parietal forms a wide rounded process interposed between the frontals. A rostral extension of the parietal has been observed in most lambeosaurines, including *Amurosauros riabinini* (AEHM 1/232), *Sahaliyana elunchunorum* (GMH W453), *Jaxartosaurus aralensis* (PIN 1/5009), *Tsintaosaurus spinorhinus* (IVPP V725), *Lambeosaurus* sp. (Gilmore 1924), *Hypacrosaurus altispinus* (AMNH 5248), and *Corythosaurus casuarius* (AMNH 5433). The rostro-lateral processes of the parietal extend to contact the post-orbitals. Ventrally the parietal forms a straight suture with the laterosphenoid and, caudally, with the prootic. Its caudo-ventral corners are notched by articulations with the supra-occipital knobs. The rostral half of the dorsal surface of the parietal is flat. From the middle part of the bone, a strong sagittal crest rises caudally. The caudal aspect of the parietal closely resembles the condition observed in *Amurosauros riabinini* (see Godefroit et al. 2004b): the parietal forms a high triangular process that overhangs the supraoccipital and separates the

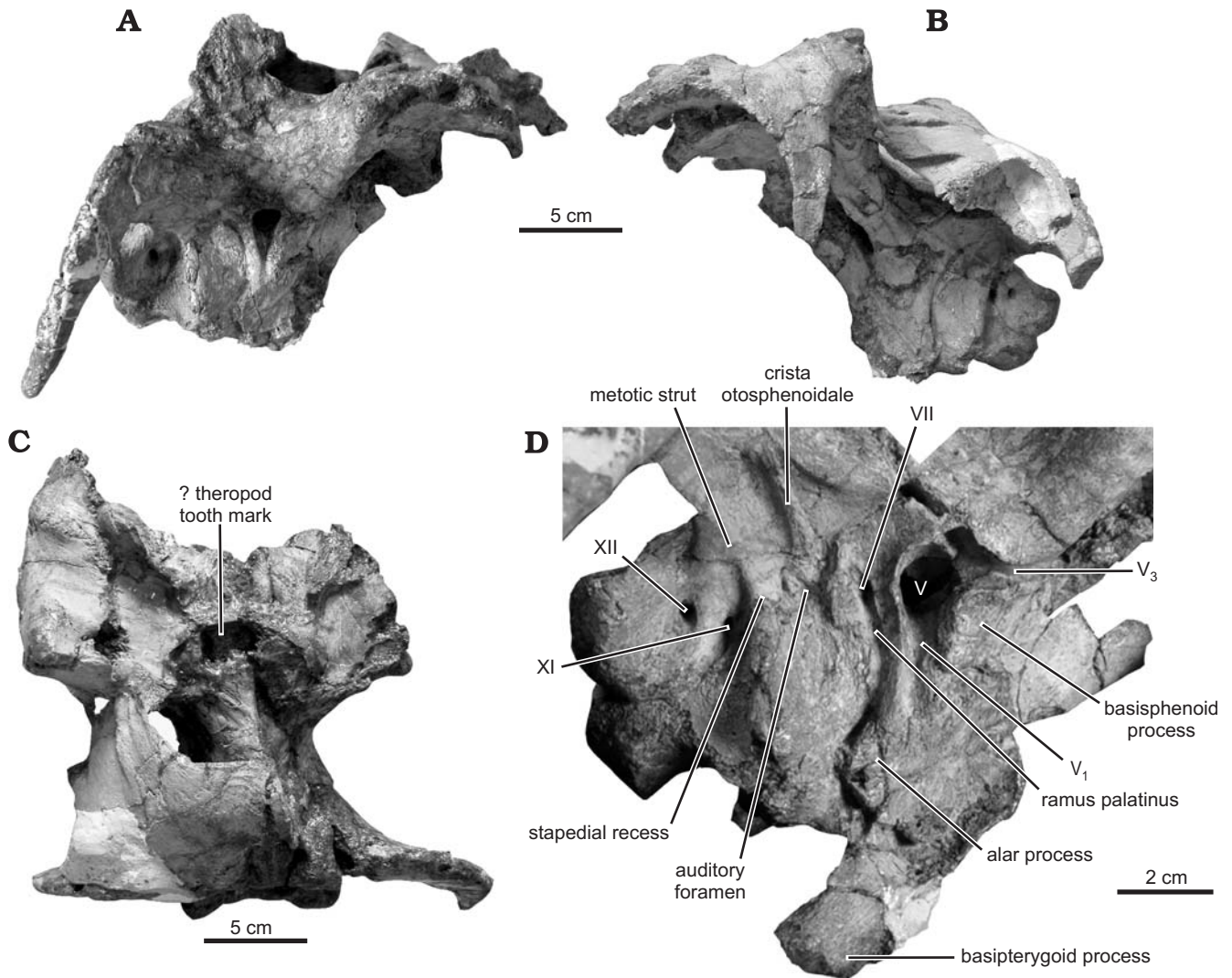


Fig. 5. Photographs of the braincase of hadrosaurid dinosaur *Olorotitan arharensis* Godefroit, Bolotsky, and Alifanov, 2003 (AEHM 2/845, holotype), from the Upper Cretaceous of Kundur (Russia), in right lateral (A), left lateral (B), and dorsal (C) views. D. Details of the right lateral view of the braincase.

squamosals from each other (Figs. 4C, E, 5A). The caudal surface of the parietal is deeply excavated and may have served as attachment area for a powerful ligamentum nuchae (Fig. 4E).

*Frontal*.—The caudal portion of the frontal of AENM 2/845 has a large rectangular perforation (Figs. 4C, 5C) that might possibly correspond to a theropod premaxillary tooth mark (see above). Although the dorsal surface of the bone is markedly crushed around this perforation, it seems that a slight frontal dome was developed at this level, as observed in numerous lambeosaurines: *Corythosaurus* (AMNH 5248), “*Procheneosaurus convincens*” (PIN 2230), “*Cheneosaurus tolmanensis*” (Lambe 1917), “*Tetragonosaurus erectofrons*” (Parks 1931; Evans et al. 2005), *Lambeosaurus magnicristatus* (Evans and Reisz 2007), *Jaxartosaurus aralensis* (PIN 5009), and *Amurosaurus riabinini* (AEHM 1/232). With an ectocranial length/width = 0.75, the frontal of AEMH 2/845 is proportionally wider than in a specimen of similar size in *Amurosaurus riabinini* (1.02 in AEHM 1/232; Godefroit et al. 2004b), but longer than in *Sahaliyanian elunchunorum* (0.6

in the holotype GMH W453). As usual in lambeosaurines, the rostral part of the dorsal surface of the frontal is highly modified to form the base of the hollow crest. It forms a broad and strongly grooved platform that slopes rostrally and maximises the area for strong attachment of the nasals and premaxillae (Figs. 4C, 5C). The frontal platform of *Olorotitan arharensis* is wider than the ectocranial part of the bone, as also observed in adult specimens of *Corythosaurus casuarius* (ROM 1940) and *Hypacrosaurus altispinus* (Gilmore 1937: fig. 32). However, it is probably an ontogenetic character: in younger *Hypacrosaurus altispinus* (AMNH 5248) and *Corythosaurus casuarius* (AMNH 5433) specimens, in which the frontals are not fused together and the median dome is well developed, the frontal platform is much narrower than the ectocranial part of the frontal. In *Amurosaurus*, on the contrary, the rostral platform is always much narrower than the caudal part of the frontal, even in older adult specimens. As in other lambeosaurines, the lateral border of the frontal of *Olorotitan arharensis* forms a thick and

interdigitate contact area, rostrally for the prefrontal and caudally for the postorbital. The frontal therefore did not participate in the dorsal margin of the orbit.

*Squamosal*.—The squamosal of *Olorotitan arharensis* is a massive element that forms the caudolateral border of the supratemporal fenestra. In lateral view, the dorsal margin of the squamosal progressively rises dorsally, so that it looks markedly concave (Figs. 4A–E, 5B, C). As usual in advanced lambeosaurines, the lateral side of the squamosal is markedly expanded above the cotylus (Figs. 4A–C, 5B, C). The rostral process of the squamosal is short but high. As previously described in *Amurosaurus riabinini* (Godefroit et al. 2004b), its lateral side has two parallel ridges that limit a wide articular surface for the caudal ramus of the postorbital (Figs. 4A, B, 5B, C). The lower ridge forms the dorsal limit of a large scar for attachment of *M. adductor mandibulae externus superficialis* (Ostrom 1961). Both the pre- and post-cotyloid processes are broken off. The postcotyloid process (Fig. 4A) is massive and mediolaterally widened. The medial ramus of the squamosal is also particularly elevated (Fig. 4E). The caudal triangular process of the parietal separates the medial rami of the paired squamosals along nearly their entire height; however, they maybe contacted each other over a short distance quite dorsally above the triangular process. The ventromedial corner of the medial ramus forms a cup-shaped articular surface for synovial articulation with the dorsal knob of the supraoccipital (Fig. 4E).

*Postorbital*.—The medial ramus of the postorbital is less shortened than in *Amurosaurus*. Its rostromedial border is particularly thick and forms a persillate articulation with the prefrontal and frontal. Because of crushing of the braincase at this level, it is unclear whether the postorbital contacts the parietal caudally. The caudal ramus of the postorbital is shorter, straighter and higher than in *Amurosaurus riabinini* (Figs. 4B, 5B). Shortening of the caudal ramus is of course correlated with the general shortening of the parietal and of the supratemporal fenestra. Although the caudal ramus of the left postorbital is crushed and the squamosal displaced, it seems that the dorsal margin of the infratemporal fenestra lay slightly below the level of the dorsal margin of the orbit (contra Prieto-Marquez 2010a), as observed in lambeosaurines except *Aralosaurus tuberiferus*, *Jaxartosaurus aralensis*, and *Tsintaosaurus spinorhinus* (Prieto-Marquez 2010a; character 192). It must be noted that the dorsal margin of the supratemporal fenestra was apparently substantially more dorsally located than the dorsal margin of the orbit in *Amurosaurus riabinini* (contra Prieto-Marquez 2010a).

The ventral ramus of the postorbital is rather slender and triangular in cross-section (Figs. 4B, 5B). Its caudal side is deeply excavated, along its whole height, by the articulation facet for the ascending process of the jugal. The dorsolateral orbital rim is rugose, as observed in other hadrosaurids (Maryńska and Osmólska 1979).

There is no trace of a dorsal promontorium, as described by Godefroit et al. (2001) in *Charonosaurus jiyinensis*: in

this taxon, the sutural surface for the prefrontal clearly extends onto the dorsal surface of the postorbital, forming an elongated, thickened, and rugose area that helped supporting the supracranial crest. Sullivan and Williamson (1999: figs. 16B, 17B) indicated that, in *Parasaurolophus tubicen*, the postorbital meets the prefrontal with a thickened, rugose contact. For that reason, Godefroit et al. (2001) hypothesized that the dorsal promontorium of the postorbital is a synapomorphy for *Charonosaurus* and *Parasaurolophus*. However, Evans et al. (2007) noted that the presence or absence of this character could not be verified on close inspection of the *P. cyrtocristatus* and *P. walkeri* holotype skulls. Therefore, the phylogenetic importance of this character remains doubtful. Prieto-Marquez (2010a; character 128) subsequently gave another definition for the dorsal promontorium of the postorbital: when the dorsal promontorium is present, the articular margin of the prefrontal is elevated and the dorsal surface of the postorbital above the jugal process is deeply depressed. Following this latter definition, a dorsal promontorium can be identified in *Olorotitan arharensis* and is also present in *Amurosaurus riabinini* and in all North American lambeosaurines.

*Prefrontal*.—Only a small portion of the prefrontal is preserved in AEHM 2/845. It is inserted between the frontal and the postorbital (Fig. 4C). As in *Corythosaurus casuarius* (AMNH 5433) and *Hypacrosaurus altispinus* (AMNH 5248), the prefrontal is much less developed medially in *Olorotitan arharensis* than in *Amurosaurus riabinini* and *Jaxartosaurus aralensis* and only participates in a small part of the ventral articulation platform for the hollow crest, although it forms the greatest part of this platform in the latter two taxa (Godefroit et al. 2004b).

*Maxilla*.—In lateral view, the rostral part of the ventral margin is not straight, as in most hadrosaurids, but distinctly down-turned, as is also the case in *Tsintaosaurus spinorhinus* and *Lambeosaurus laticaudus*. The dorsal process is directed caudodorsally from the horizontal alveolar ramus; its apex lies at the level of the caudal third of the bone and the maxilla therefore looks strongly asymmetrical in lateral view (Fig. 6). The jugal process forms a concave surface that nearly covers laterally the whole height of the dorsal process (Fig. 6A<sub>1</sub>). The dorsal process is proportionally higher and rostrocaudally shorter than in other lambeosaurines, in relation to the high and short rostral process of the jugal. The lacrimal facet forms a deep elongated groove along the rostrolateral side of the dorsal process. At its base, a large ovoid canal, which probably represents the antorbital fenestra among hadrosaurids (Weishampel and Horner 1990), penetrates the dorsal process to communicate with its excavated caudomedial surface. Ventral to the jugal process, six foramina penetrate the maxilla and extend caudodorsally to open into the excavated caudomedial surface of the dorsal process, caudal to the antorbital foramen. As is usual in hadrosaurids, the ectopterygoid ridge is strongly developed and nearly horizontal; only its distal part is ventrally deflected (Fig. 6A). As

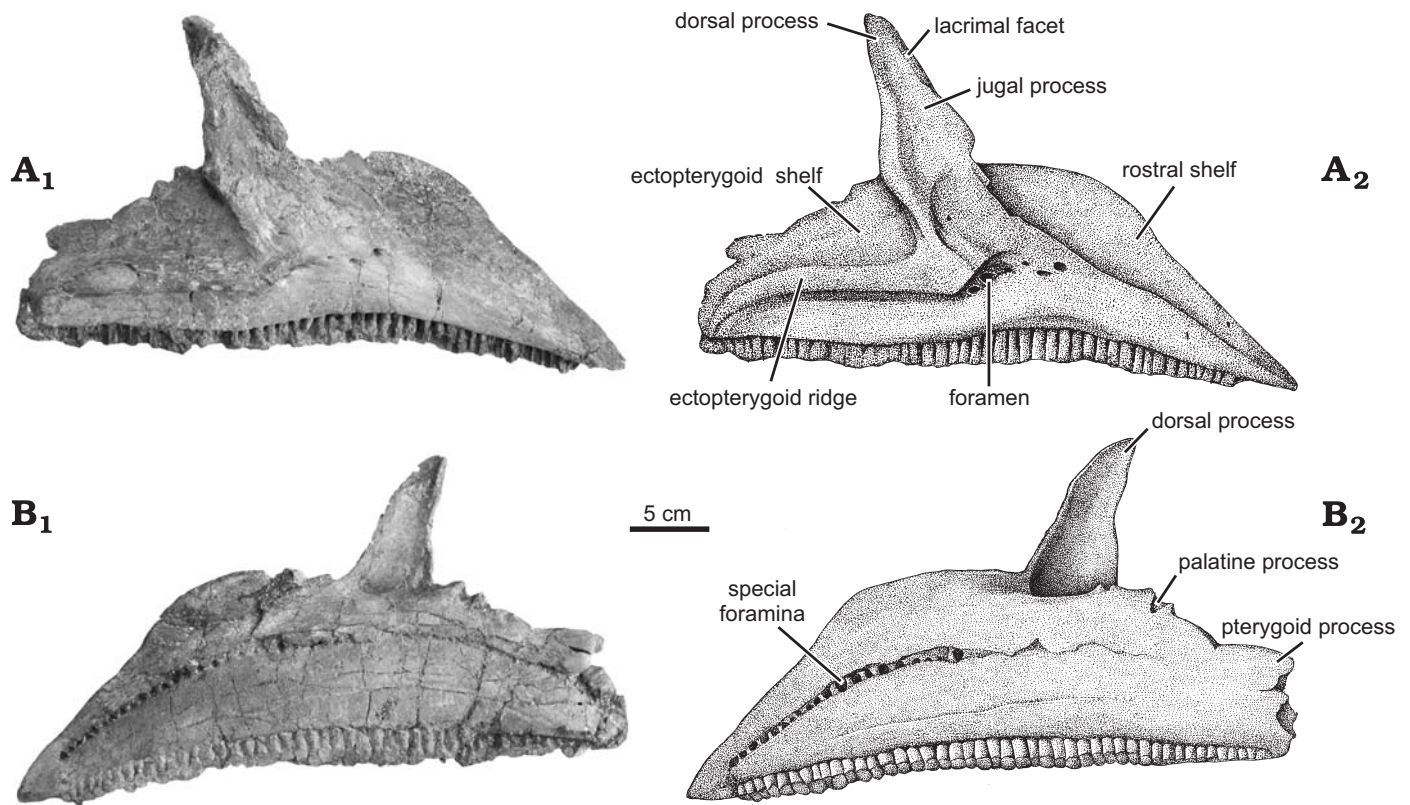


Fig. 6. Right maxilla of hadrosaurid dinosaur *Olorotitan arharensis* Godefroit, Bolotsky, and Alifanov, 2003 (AEHM 2/845, holotype), from the Upper Cretaceous of Kundur (Russia), in lateral (A) and medial (B) views. Photographs (A<sub>1</sub>, B<sub>1</sub>), explanatory drawings (A<sub>2</sub>, B<sub>2</sub>).

is usual in Euhadrosauria (sensu Weishampel et al. 1993), the ectopterygoid ridge extends to the jugal facet as a continuous, albeit recurved lip, but the maxilla-jugal joint is not set much higher than the ectopterygoid ridge, contrasting with the condition described in *Tsintaosaurus spinorhinus* and *Pararhabdodon isonensis* (Prieto-Marquez and Wagner 2009). The ectopterygoid shelf is broader than in *Amurosaurus riabinini*. Caudal to the dorsal process, it forms a triangular palatine process that slopes inwards and whose caudal border has a distinct articular facet for the palatine. More caudally, the medial edge of the ectopterygoid shelf forms a caudally-directed pterygoid process, which received the maxillary process of the pterygoid (Fig. 6B). The rostral shelf of the maxilla, which supported the lateral premaxillary process, is much better developed than in *Amurosaurus riabinini*. The medial surface of the maxilla is perfectly flat and pierced by a series of special foramina interconnected by a gently curving horizontal groove, along the whole length of the bone (Fig. 6B).

There are about 45 rows of maxillary teeth in the holotype specimen. The crowns are narrow, lanceolate, perfectly straight and symmetrical. The median primary ridge is more salient than on the dentary teeth. There is no secondary ridge. Both margins of the crowns are gently denticulate. The marginal denticulations are apparently simple. The roots are high and very narrow.

*Jugal*.—The rostral process is extremely shortened rostro-caudally but dorsoventrally expanded. Its rostral border is perfectly straight and slightly caudodorsally inclined in lateral view (Fig. 7). The shape of the rostral process in *Olorotitan arharensis* approaches the condition observed in jugals that may tentatively be referred to *Tsintaosaurus spinorhinus* (Young 1958: fig. 41). It also resembles the rostral processes described in *Hypacrosaurus altispinus* (Evans 2010), although the rostral process appears less shortened in these North American lambeosaurines. In *Amurosaurus riabinini* (Godefroit et al. 2004b), *Sahaliyanian elunchunorum* (Godefroit et al. 2008), *Charonosaurus jiyinensis* (Godefroit et al. 2001), *Lambeosaurus lambei*, *Corythosaurus casuarius*, and *Hypacrosaurus stebingeri* (Evans 2010), the rostral process tends to be broader with a distinctly more rounded profile, particularly in juveniles. On the medial side of the rostral process, the maxillary facet is narrow, rectangular in shape, and strongly striated for tight ligamentous attachment with the maxilla. Because of the shortening of the rostral process, the maxillary process is nearly vertical. The lacrimal process is particularly high, too. The jugal neck is strongly contracted, and the ventral margin of the bone, particularly concave. The postorbital process is thin and appears higher than in other lambeosaurines: the ratio “height of jugal at the level of postorbital process/length of jugal” = 1. The lacrimal and postorbital processes of the

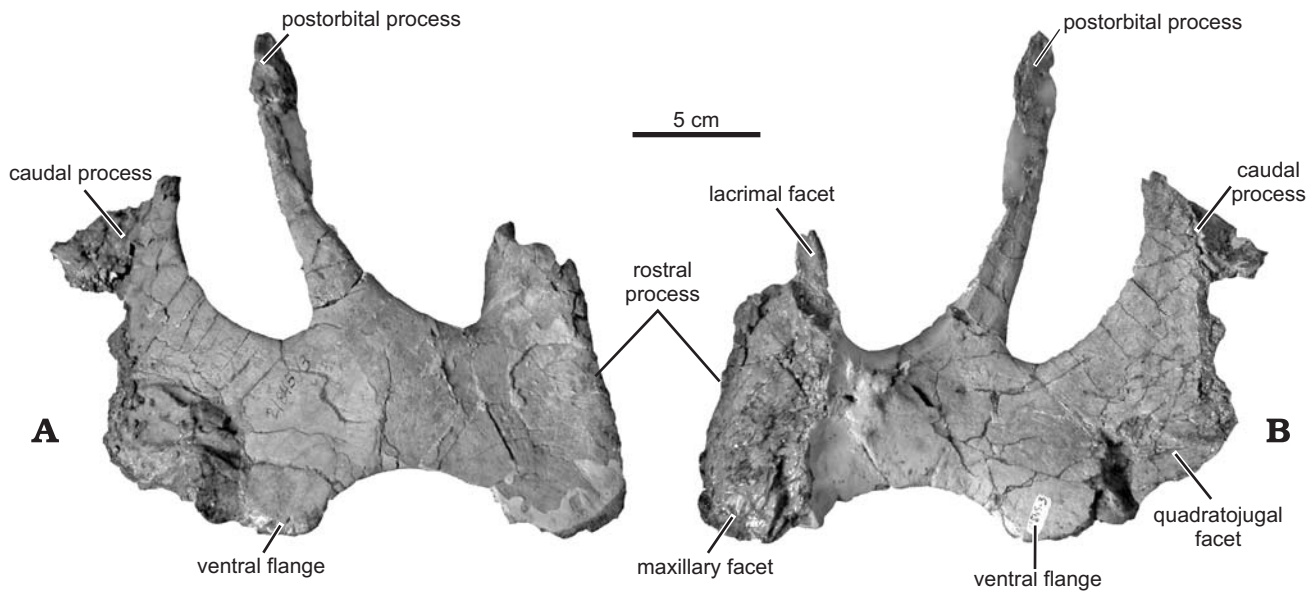


Fig. 7. Right jugal of hadrosaurid dinosaur *Olorotitan arharensis* Godefroit, Bolotsky, and Alifanov, 2003 (AEHM 2/845, holotype), from the Upper Cretaceous of Kundur (Russia), in lateral (A) and medial (B) views.

jugal are nearly parallel, indicating that the ventral part of the orbit was very narrow. The caudal process (or subtemporal blade) of the jugal also raises caudodorsally at about the same angle as the postorbital process, a condition also observed in *Velafrons coahuilensis* (Gates et al. 2007), *Hypacrosaurus altispinus*, and *Hypacrosaurus stebingeri* (Evans 2010), indicating that the ventral portion of the infratemporal fenestra was constricted. The caudomedial side of the caudal process has a smooth articular facet for the quadratojugal (Fig. 7B). The ventral flange is less developed than in *Sahaliyanina elunchunorum* (Godefroit et al. 2008) and *Hypacrosaurus altispinus* (Evans 2010).

**Quadrate.**—The dorsal part of the right quadrate is preserved in the holotype specimen. In lateral view, it is distinctly curved backwards, as normal in lambeosaurines. However, it appears particularly gracile, when compared with that of other lambeosaurines, such as *Amurosaurus riabinini* and *Sahaliyanina elunchunorum*. The quadratojugal notch is elongated and a continuous depressed area surrounds its lateral side, showing that it was completely covered by the quadratojugal. The pterygoid wing is particularly thick.

**Premaxilla.**—The hypertrophied premaxilla forms the expanded rostrum of the muzzle and participates in a great portion of the hollow supracranial crest. Because of the important post-mortem crushing of the crest, only the external aspect of the premaxilla can be described. The internal anatomy cannot be interpreted by C-T scanning. In lateral view, the premaxilla has a shallowly concave profile (crest-snout angle not less than  $150^\circ$ ; Fig. 8A), as in *Hypacrosaurus altispinus* and *Hypacrosaurus stebingeri* (Evans 2010). In *Corythosaurus casuarius* and *Lambeosaurus* spp., the crest-snout angle becomes progressively smaller through ontogeny and the crest-snout angle in adults does not exceed  $135^\circ$

in *Corythosaurus* and  $116^\circ$  in *Lambeosaurus* (Dodson 1975; Evans 2010). The rostral part of the premaxilla gently flares to form an arcuate beak, but the lateral expansion of the beak is limited. As described by Horner et al. (2004), the premaxillary rostral margin has a “double layer” morphology, consisting of an external rugose and denticulate layer and an internal palatal layer of thickened bone separated from the denticulate layer by a deep arcuate sulcus. As it is usual in lambeosaurines, there is no premaxillary foramen. The external naris is entirely surrounded by the premaxilla and the left and right external passages are completely separated in the snout region.

The external naris is fairly large and overhangs the rostral part of the maxilla. It is lacrimiform in shape and caudally constricted both by a ventral expansion of the caudodorsal premaxillary process and by the dorsal expansion of the caudolateral premaxillary process (Fig. 8A). Behind the external naris, both caudal processes are intimately connected into a straight suture. The caudolateral and caudodorsal processes are not separated caudally by a rostroventral process from the nasal, particularly well developed in *Corythosaurus casuarius* and in *Hypacrosaurus stebingeri*. The caudolateral process is long and extends caudally well beyond the level of the prefrontal. It forms a well developed ventrolateral articulation facet for the prefrontal. Behind this articulation, the ventral border of the caudolateral process articulates with the rostral part of the nasal. The caudal portion of the caudolateral process does not expand dorsoventrally in the frontal region of the skull and does not display a bilobate aspect, as observed in *Hypacrosaurus altispinus*, *Hypacrosaurus stebingeri*, *Lambeosaurus lambei*, *Lambeosaurus magnicristatus*, and to a lesser degree *Corythosaurus casuarius*. The caudodorsal process extends caudodorsally far beyond the level of the caudolateral process and tapers caudally into a

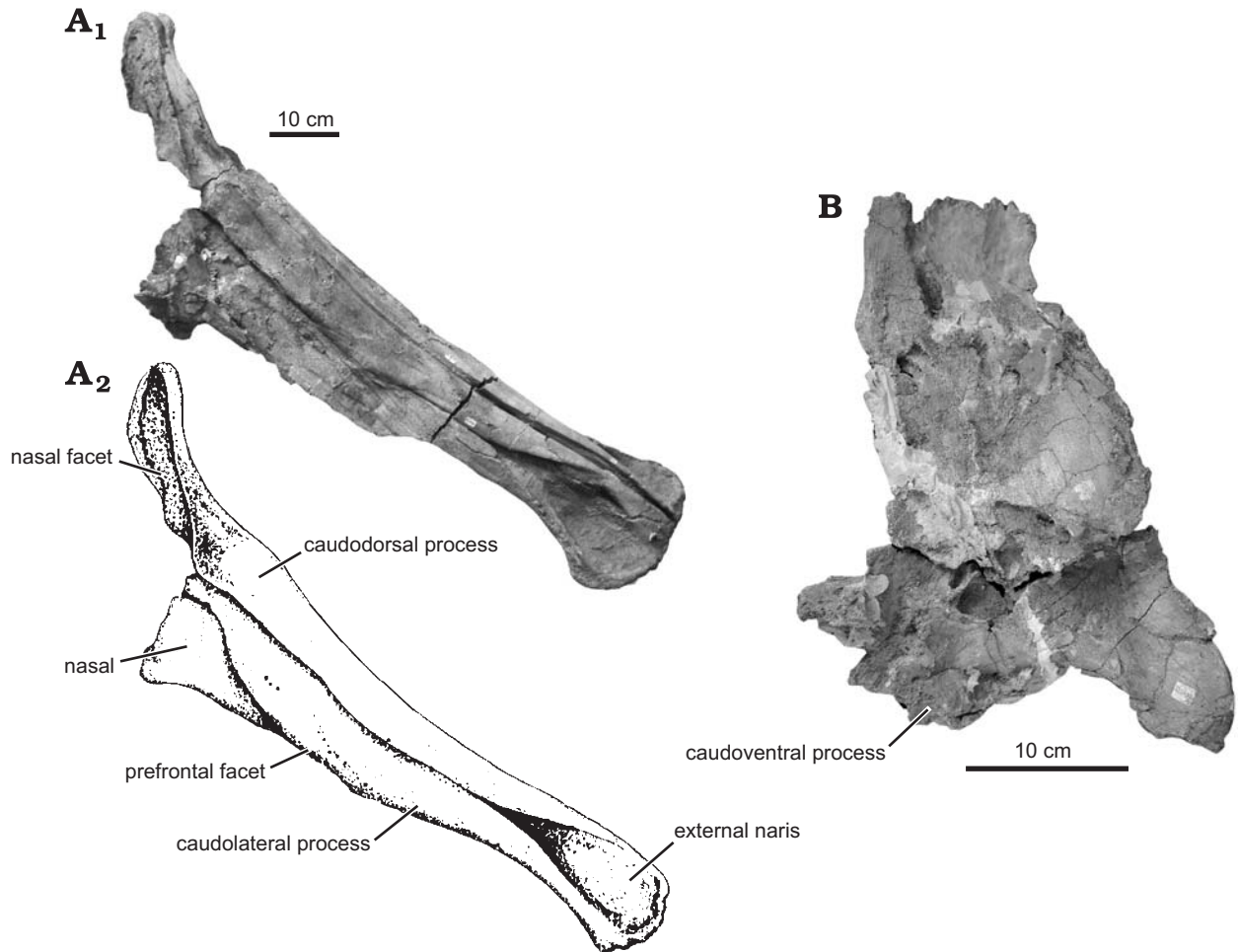


Fig. 8. Hadrosaurid dinosaur *Olorotitan arharensis* Godefroit, Bolotsky, and Alifanov, 2003 (AEHM 2/845, holotype), from the Upper Cretaceous of Kundur (Russia). **A.** Right premaxilla and rostral portion of right nasal, in lateral view. Photograph (A<sub>1</sub>), explanatory drawing (A<sub>2</sub>). **B.** Caudoventral portion of right nasal, in lateral view.

blunt point. It has no accessory rostroventral flange that overlaps the lateral surface of the nasal in the rostral region of the crest, contrasting with the condition in *Hypacrosaurus altispinus*, *Lambeosaurus lambei*, and *Lambeosaurus magnicristatus*. The caudodorsal process forms a wide ventromedial surface for extensive articulation with the nasal. This process did not participate in the caudal margin of the hollow crest, contrasting with the condition observed in *Lambeosaurus lambei* and *Lambeosaurus magnicristatus*. Caudally, the dorsolateral surface of the caudodorsal process is depressed along the midline.

**Nasal.**—Only a small part of the nasal remains attached along the ventral border of the premaxillary caudolateral process (Fig. 8A). The largest part of the bone was displaced and completely crushed. However, it can be assumed that the paired nasals formed a large fan-shaped plate, with a long external internasal joint along the caudal and caudoventral margin of the crest. The ventral margin was apparently shallowly concave and the caudoventral process, prominent (Fig. 8B). The sutural pattern with the premaxilla was apparently quite simple: rostrally, the nasal was attached caudoventrally to

the caudolateral premaxillary process, then to the caudo-dorsal process, more caudally.

**Prementary.**—The prementary of *Olorotitan arharensis* is gracile and shovel-shaped. It appears much more transversely expanded than long (Fig. 9). Because it is dorsoventrally crushed and the ends of the lateral processes are missing, its depth/length ratio (sensu Prieto-Marquez 2010a; character 23) cannot be adequately estimated. Its rostral process is perfectly straight, as in *Tsintaosaurus spinorhinus*, and forms angles of about 40° with the dorsal margin of the lateral processes. The rostral margin is strongly denticulate, with 13 subrectangular denticles that project rostrally. The denticles are tightly arranged and there is no substantial separation between their bases. A dozen nutrient foramina are distributed across the entire rostral margin. Two pairs of median processes extend back over the dentary symphysis. The dorsal pair is longer and spike-like; it extends along the rostral process as a sharp ridge. The ventral pair of median processes is shorter, but wider. It is supported on a continuous ridge along the caudal margin of the prementary. High dorsal ridges extend along the lateral processes.

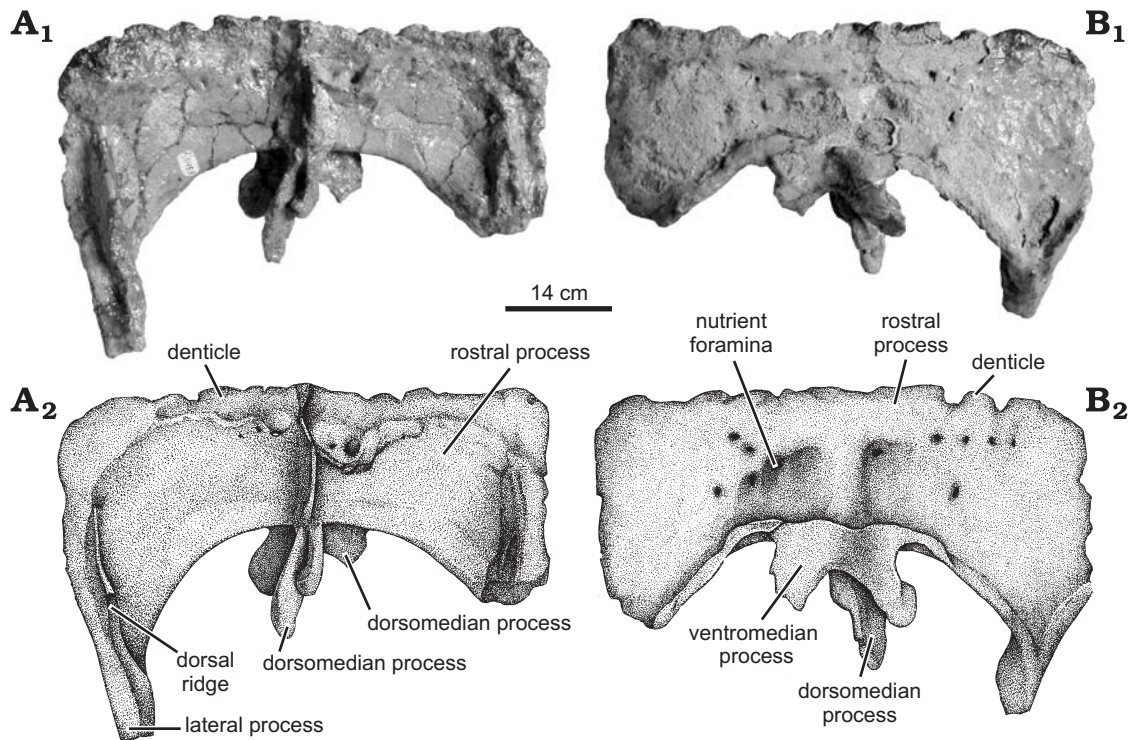


Fig. 9. Predentary of hadrosaurid dinosaur *Olorotitan arharensis* Godefroit, Bolotsky, and Alifanov, 2003 (AEHM 2/845, holotype), from the Upper Cretaceous of Kundur (Russia), in dorsal (A) and ventral (B) views. Photographs (A<sub>1</sub>, B<sub>1</sub>), explanatory drawings (A<sub>2</sub>, B<sub>2</sub>).

**Dentary.**—In dorsal view, the dentary appears less curved externally than in *Charonosaurus jiyinensis* (Fig. 10C). In lateral view (Fig. 10B), the ventral deflection of the rostral part of the dentary is less important than in specimens of comparable size that can be attributed to *Sahaliyana elunchunorum*, *Amurosaurus riabinini*, and *Tsintaosaurus spinorhinus*. It more closely resembles the condition in *Charonosaurus jiyinensis* and in North American lambeosaurines (see Godefroit et al. 2001), although considerable variation can be observed in North American taxa such as *Corythosaurus* and *Lambeosaurus*. The rostral ventral border of the dentary forms an angle of about 20° with the horizontal. The ventral deflection originates near the rostral third of the dental battery. The dental battery is long, formed by about 38 tooth rows in the holotype (Fig. 10A). The ratio between the length of the diastema (“proximalmost edentulous slope” of Prieto-Marquez 2010a) and the distance between the rostralmost tooth position and the caudal margin of the coronoid process is 0.27, exactly as in AEMH 1/19, the holotype of *Amurosaurus riabinini*. The diastema appears slightly shorter in *Sahaliyana elunchunorum* (0.24 in GMH W451; contra Prieto Marquez [2010a], who considered that a ratio between 0.32 and 0.45 is synapomorphic for *Amurosaurus* and *Sahaliyana*). The diastema forms an angle of about 165° with the horizontal. According to Prieto-Marquez (2010a; character 34), an angle between the diastema and the horizontal of 150° or more is synapomorphic for *Corythosaurus casuarius*, *Lambeosaurus lambei*, *Lambeosaurus magnicristatus*, *Hypacrosaurus stebingeri*, and *Velafrons coahuilensis*. However, this character is not retained in the present

phylogenetic analysis, because its polarity remains controversial (1 in *Bactrosaurus johnsoni* and *Probactrosaurus* ssp, according to Prieto-Márquez 2008: table A.1). The rostral articular surface for the predentary is typically scoop-shaped (Fig. 10C). The dentary symphysis is nearly horizontal (Fig. 10A). The lingual projection of the symphyseal region (ratio between the labiolingual extension of the symphyseal region and the maximum labiolingual width of the dentary ramus [Prieto-Marquez 2010a; character 38] = 2.25) is not as important as in *Tsintaosaurus spinorhinus* and *Pararhabdodon isonensis* (Prieto-Marquez and Wagner 2009). The lateral side of the dentary is regularly convex dorsoventrally. It is irregularly pierced by half a dozen foramina for vessels and nerves. The coronoid process is robust, but appears proportionally lower than in *Sahaliyana elunchunorum* and *Amurosaurus riabinini*. As is usual in hadrosaurids, it slopes rostrally and is slightly curved medially; its lateral side has an extended triangular surface along its dorsal part, marking the insertion of a powerful *M. pseudotemporalis*. In caudal view, the dentary is deeply excavated by the adductor fossa. Contrary to what is usually observed in hadrosaurids, the mandibular groove is closed medially (Fig. 10A). However, an open mandibular groove can be observed in other, smaller lambeosaurines dentaries discovered at Kundur. Therefore, this unusual condition in AEHM 2/845 may be pathological, or an ontogenetic character, observed in older individuals only. The angular facet is elongated along the medioventral border of the dentary (Fig. 10A).

Two or three efficient teeth plus two or three replacement teeth form each dentary tooth row (Fig. 10A). The replace-

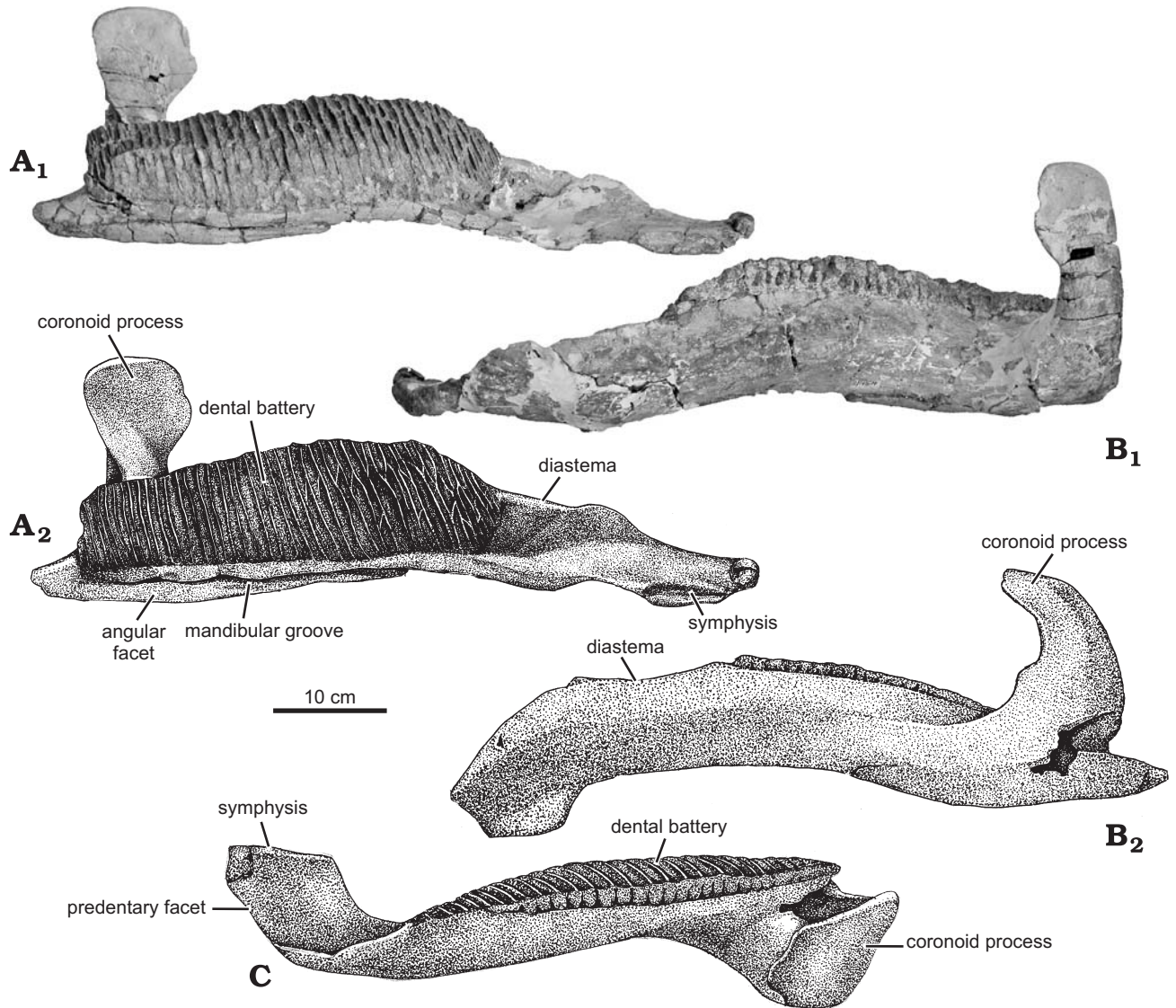


Fig. 10. Left dentary of hadrosaurid dinosaur *Olorotitan arharensis* Godefroit, Bolotsky, and Alifanov, 2003 (AEHM 2/845, holotype), from the Upper Cretaceous of Kundur (Russia), in medial (A), lateral (B), and dorsal (C) views. Photographs (A<sub>1</sub>, B<sub>1</sub>), explanatory drawings (A<sub>2</sub>, B<sub>2</sub>, C).

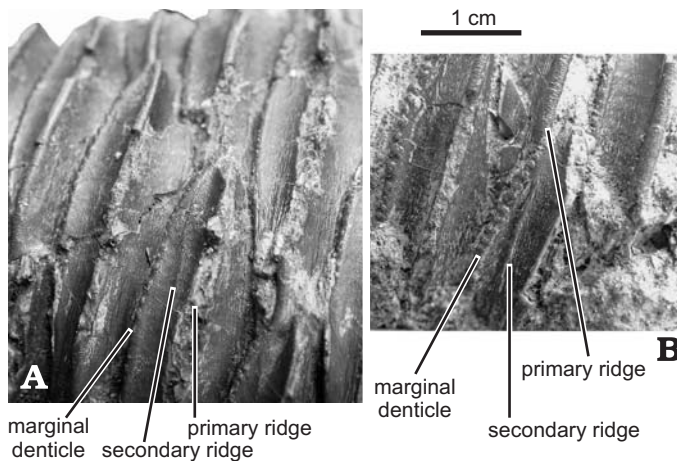


Fig. 11. Right dentary teeth of hadrosaurid dinosaur *Olorotitan arharensis* Godefroit, Bolotsky, and Alifanov, 2003 (AEHM 2/845, holotype), from the Upper Cretaceous of Kundur (Russia), in lingual views. **A**. From the middle part of the dental battery. **B**. From the caudal part of the dental battery.

ment pattern is normal (Ostrom 1961), with caudal teeth progressively more completely erupted. The dentary crowns are lanceolate. Their enamelled side is proportionally wider than in the maxillary teeth, with a “height/width” ratio of about 4 for the teeth located in the middle of the dental battery (Fig. 11). The median carina is prominent and sometimes slightly sinuous, especially on the rostral teeth, a character that is often observed in lambeosaurines (Godefroit et al. 2001). One, and sometimes even two, faint mesial accessory ridges are sporadically developed on some crowns. The marginal denticles are well developed along the dorsal half of the mesial margin of the crown, each denticle consisting of three separate and rounded knobs aligned labiolongually. Because the distal margin of the crown is covered by the mesial margin of the succeeding one, the development of the distal marginal denticles cannot be accurately assessed.

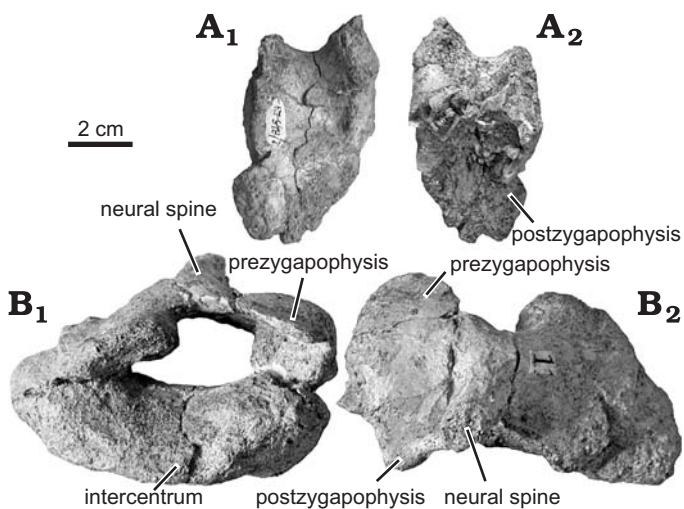


Fig. 12. Hadrosaurid dinosaur *Olorotitan arharensis* Godefroit, Bolotsky, and Alifanov, 2003 (AEHM 2/845, holotype), from the Upper Cretaceous of Kundur (Russia). A. Left proatlas, in dorsal (A<sub>1</sub>) and ventral (A<sub>2</sub>) views. B. Atlas, in cranial (B<sub>1</sub>) and dorsal (B<sub>2</sub>) views.

*Surangular*.—Both surangulars are partly preserved in AEHM 2/845. They are identical to those in other lambeosaurines and therefore they are not described here.

#### Axial skeleton

*Cervical vertebrae*.—The articulated cervical series of AEHM 2/845 comprises 18 vertebrae, which means that the neck was more elongated than in any other hadrosaurid. In hadrosaurines, the cervical series is composed of 12 or 13 vertebrae (Lull and Wright 1942). Fifteen cervical vertebrae are reported in *Lambeosaurus magnicristatus* (Evans and Reisz 2007), 14 in a juvenile specimen of *Lambeosaurus ?lambei* (Lull and Wright 1942), and 13 in *Parasaurolophus walkeri* (Gilmore 1924).

*Proatlas*.—A flattened bone, found close to the proximal end of the cervical series, is tentatively interpreted as a left proatlas, by comparison with that described in *Mantellisaurus atherfieldensis* (Norman 1986: figs. 23, 24). However that bone, appears proportionally much larger in *Olorotitan* than in *Mantellisaurus*. It is roughly triangular, and the apex is caudal (Fig. 12A). The cranial border is shallowly concave. A large ventromedially directed articular facet is effectively the postzygapophysis of the proatlas (Norman 1986).

*Atlas*.—The atlas is composed of an intercentrum, fused neural arches, and an odontoid. In anterior view, the intercentrum is crescentic and particularly enlarged transversely (Fig. 12B<sub>1</sub>). Its rostral surface is inclined and it forms a wide and flattened articulation surface with the occipital condyle. Its posterior surface, which articulated with the axis complex, is vertical and flat. Its dorsolateral corners are truncated by the articular facets for the neural arch.

The neural arches are completely fused in this specimen and form a low, caudally inclined neural spine (Fig. 12B). Their cranial borders form very wide prezygapophyseal pro-

cesses that supported each proatlas. The postzygapophyseal processes are also widely developed on the caudal side of the neural arches, overlying the prezygapophyses of the axis (Fig. 12B<sub>2</sub>).

The odontoid is massive and crescentic (Fig. 13A). Its dorsal side, which forms the floor of the neural canal, is slightly concave transversely, whereas its ventral side is very convex. The odontoid is completely fused to the axial centrum.

*Axis*.—The axial centrum is poorly preserved and its limits with the odontoid process and the axial intercentrum cannot be discerned (Fig. 13A). It appears relatively elongated, slightly expanded laterally at both ends. The axial intercentrum is crescentic in shape along the cranioventral side of the centrum. The widely developed prezygapophyses correspond in shape to the atlantal postzygapophysis, and extend cranially beyond the margin of the neural spine and centrum. The neural arch forms a large, craniocaudally expanded, and regularly convex neural spine (Fig. 13A). Caudally, the spine bifurcates into two divergent laminae that support ventrally the broad elliptical postzygapophyses (Fig. 13B). Directly caudal to the prezygapophyseal peduncle, small short transverse processes project caudolaterally from the lateral sides of the neural arch and terminate into smoothly rounded diapophysis.

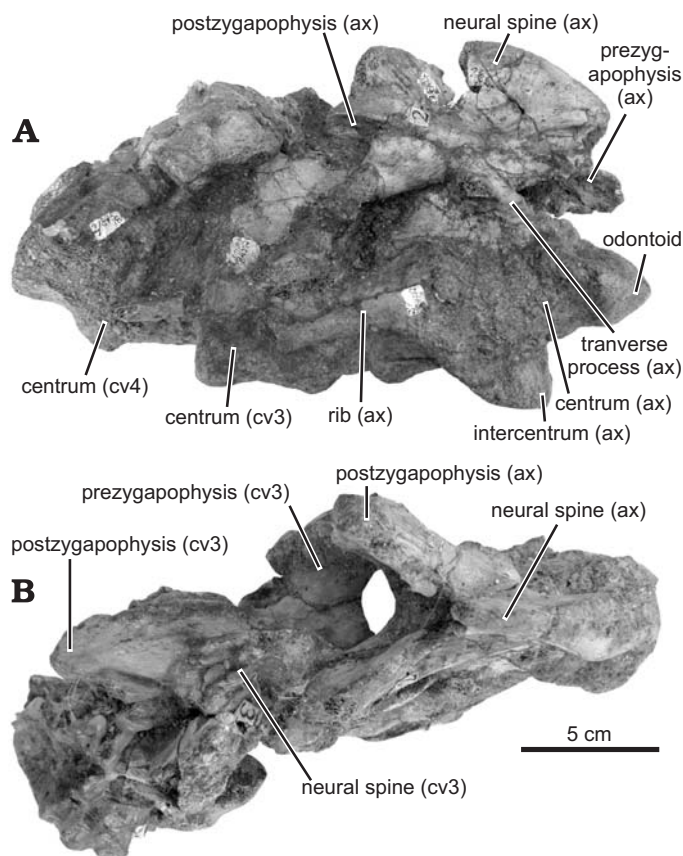


Fig. 13. Axis complex and cervical vertebrae 3–4 of hadrosaurid dinosaur *Olorotitan arharensis* Godefroit, Bolotsky, and Alifanov 2003 (AEHM 2/845, holotype), from the Upper Cretaceous of Kundur (Russia), in right lateral (A) and dorsal (B) views. Abbreviations: ax, axis; cv, cervical vertebra.

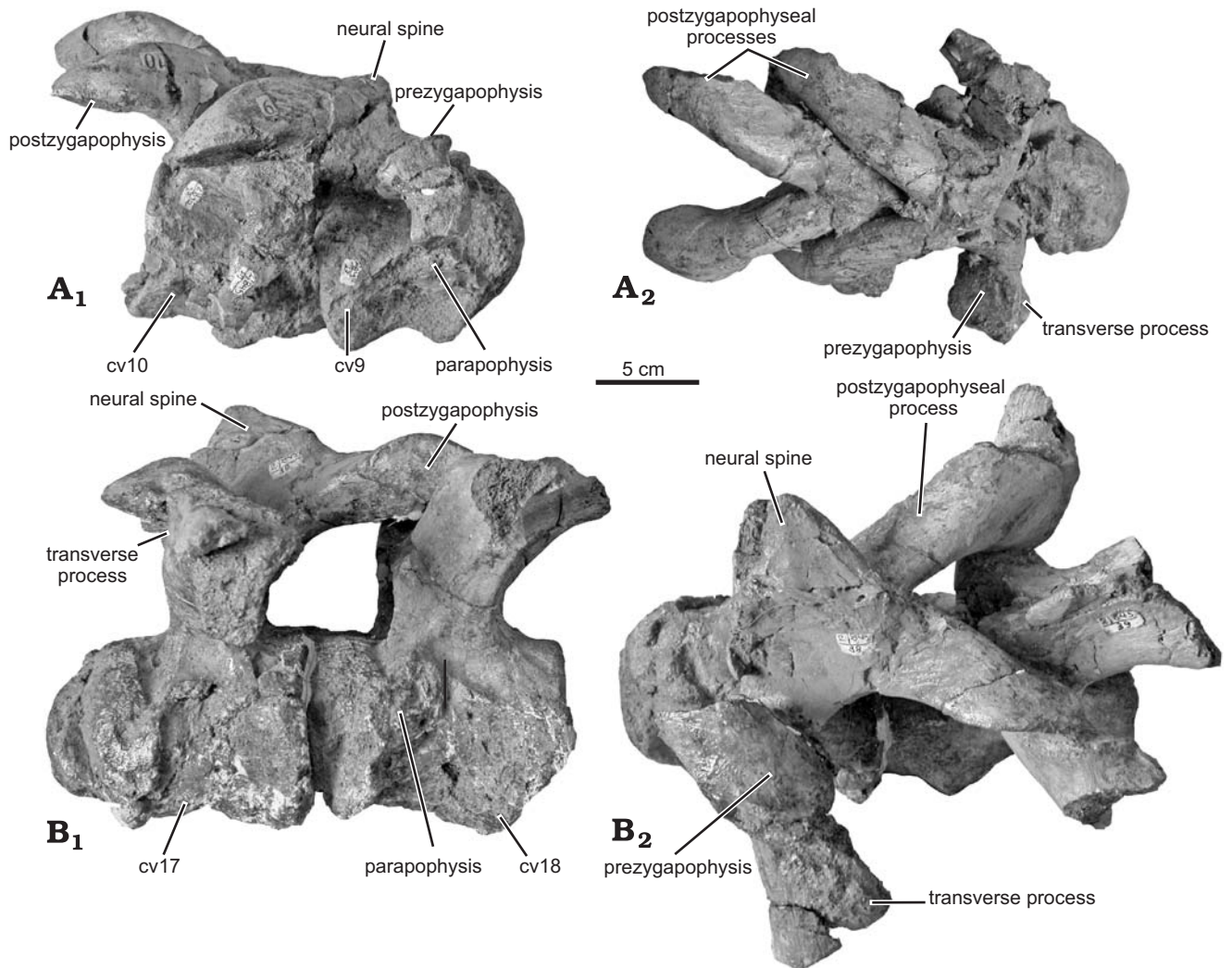


Fig. 14. Cervical vertebrae of hadrosaurid dinosaur *Olorotitan arharensis* Godefroit, Bolotsky, and Alifanov 2003 (AEHM 2/845, holotype), from the Upper Cretaceous of Kundur (Russia). **A.** Cervical vertebrae 9–10, in right lateral (**A<sub>1</sub>**) and dorsal (**A<sub>2</sub>**) views. **B.** Cervical vertebrae 17–18, in left lateral (**B<sub>1</sub>**) and dorsal (**B<sub>2</sub>**) views. Abbreviation: cv, cervical vertebra.

*Post-axial cervical vertebrae.*—All the cervical centra are strongly opisthocoelous, with a hemispherical cranial articular surface and a deeply concave, cup-shaped caudal surface (Fig. 14). Because of post-mortem deformation and intimate articulation between adjacent opisthocoelous centra, the vertebrae cannot be adequately measured. However, it can be asserted that all the cervical centra are higher than wide and that their length tends to increase slightly throughout the cervical series ( $L = 100$  mm in C4, 118 mm in C17). All the cervical centra are wider caudally than cranially and are slightly contracted in the middle. All have a prominent ventral keel: the rostral and caudal articular surfaces therefore retain a characteristic heart shape; above the keel, the lateral walls are slightly concave and may be pierced by a small nutritive foramen. On the cranial cervical vertebrae, the parapophysis is set on the cranial end of a horizontal ridge, in the middle of the lateral side of the centrum; towards the caudal part of the neck, the parapophyses progressively migrate towards the dorsolateral side of the centrum, at the base of the transverse processes of the neu-

ral arch. The neural arch encloses a wide neural canal. On Cv3 and Cv4, the transverse processes are only poorly developed, but their size progressively increases throughout the series: they become longer, stouter and more curved ventrally and caudally (Fig. 14B<sub>2</sub>). The elliptical diapophysis is set on the lateral end of the transverse process. The articular surface of the prezygapophysis is inclined caudally and slightly medially on the dorsal side of the transverse process (Fig. 14A, B<sub>2</sub>). The postzygapophyseal processes are particularly long and stout in *Olorotitan arharensis*, more than three times longer than the width of the neural arch (Fig. 14A<sub>2</sub>, B<sub>2</sub>). They diverge caudally to cover the transverse processes of the succeeding adjacent vertebra. The large and elliptical postzygapophyses are inclined cranially and slightly laterally (Fig. 14A<sub>1</sub>, B<sub>1</sub>). The postzygapophyseal processes become progressively larger passing through the cervical series, and the maximal size is reached in Cv16. Along the cervical series, the bases of the postzygapophyseal processes tend to fuse together, so that they become higher and less divergent. The neural spine forms

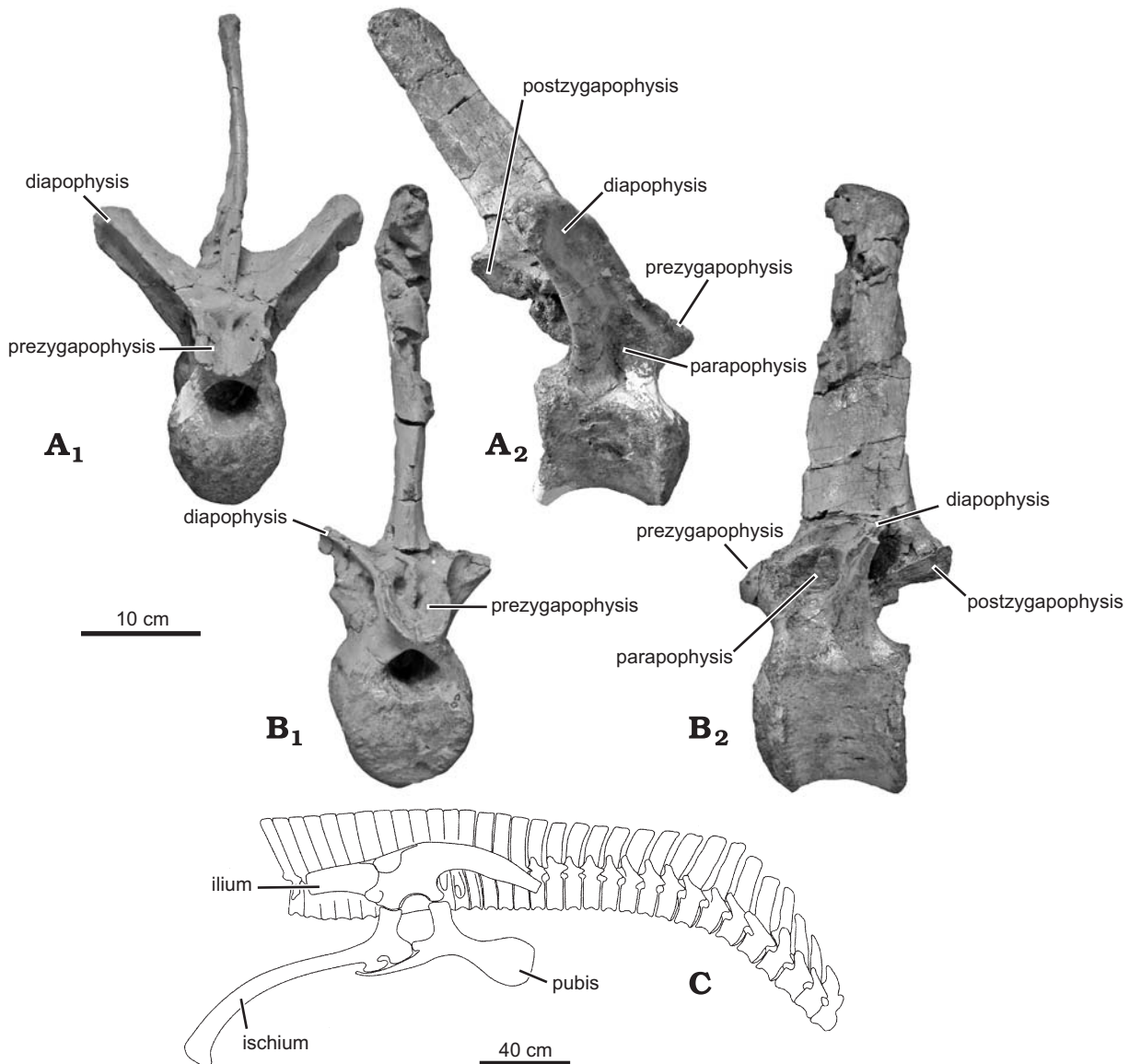


Fig. 15. Hadrosaurid dinosaur *Olorotitan arharensis* Godefroit, Bolotsky, and Alifanov, 2003 (AEHM 2/845, holotype), from the Upper Cretaceous of Kundur (Russia). **A.** Cranial dorsal vertebra, in cranial (**A<sub>1</sub>**) and right lateral (**A<sub>2</sub>**) views. **B.** Caudal dorsal vertebra, in cranial (**B<sub>1</sub>**) and left lateral (**B<sub>2</sub>**) views. **C.** Reconstruction of the articulated dorsal series, sacrum, and right pelvic girdle in right lateral view.

a small tubercle between the postzygapophyseal processes. It is slightly better developed on Cv17 and Cv18, forming a small hook-like process (Fig. 14B).

**Cervical ribs.**—Cervical ribs are poorly preserved in the holotype. The axial rib is apparently double-headed (Fig. 13A), as are the other cervical ribs. The capitulum articulates with the parapophysis on the lateral surface of the centrum and the tubercle meets the diapophysis on the distal end of the transverse process. The capitulum and tuberculum become relatively longer in the caudal part of the cervical series. Although they are in all cases incomplete, the distal end of the cervical ribs appears mediolaterally compressed and caudoventrally oriented.

**Dorsal vertebrae.**—Thirteen dorsal vertebrae are preserved in the holotype specimen, but they were found completely

disarticulated, so their exact position along the dorsal series cannot be ascertained. The six caudalmost dorsal vertebrae are preserved in connection in the referred specimen AEHM 2/846. All the dorsal vertebrae remain distinctly opisthocoelous in *Olorotitan arharensis* (Fig. 15B, D). According to Horner et al. (2004), this is an unusual character among hadrosaurids: usually, only the first dorsal is slightly opisthocoelous, whereas the other centra are amphiplatyan. However, strongly opisthocoelous dorsal vertebrae have been described in *Amurosaurus riabinini* (Godefroit et al. 2004b) and we feel that this character must be checked in detail among North American hadrosaurids. Because of the development of the ventral ridge, the cranial and caudal articular surfaces remain heart-shaped (Fig. 15A<sub>1</sub>, B<sub>1</sub>). The centra progressively become relatively shorter through the dorsal series (Fig. 15C). Above the carina, the lateral sides of the

centrum are strongly contracted and pierced by several irregularly distributed nutritive foramina. The neural arch is very robust. The prezygapophyses are wide, with a craniocaudal long axis. They are slightly concave and are inclined medially, dorsally, and cranially. Caudodorsally, they are separated from each other by a thin median vertical ridge from the base of the neural spine and, cranioventrally, by an incision (Fig. 15A<sub>1</sub>, B<sub>1</sub>). The postzygapophyses are also wide, slightly concave, with a craniocaudal great axis; they are inclined ventrally, laterally, and slightly caudally (Fig. 15A<sub>2</sub>, B<sub>2</sub>). A deep indentation separates them at the base of the neural spine. The diapophyses are elongated and stout. They are strongly inclined caudally and dorsally. This is in apparent contradiction with Horner et al.'s (2004) assertion that the diapophyses of dorsal vertebrae are nearly horizontal in lambeosaurines. The ventral side of the diapophyses has a strong carina, extending towards the caudoventral corner of the neural arch. This carina forms the ventrolateral margin of extremely excavated fossae on the caudal side of the neural arch, below the postzygapophyses. These fossae are separated from each other by a median carina from the base of the postzygapophyses to the roof of the medullary canal. The parapophyses form slight kidney-shaped depressed areas between the diapophyses and prezygapophyses (Fig. 15A<sub>2</sub>, B<sub>2</sub>). The neural spines are subrectangular in lateral view. All are much higher than the corresponding centrum. The highest spines are about four times as high as craniocaudally long and more than three times as high as the centrum. Their apex is roughened, indicating the possible presence of a cartilage cap in life. The orientation of the neural spine is variable, depending on the position within the dorsal series: on the cranial dorsal vertebrae, it is distinctly inclined caudally (Fig. 15A<sub>2</sub>), whereas it becomes nearly vertical in the caudal part of the dorsal series (Fig. 15B<sub>2</sub>).

*Dorsal ribs.*—Only a few dorsal ribs are associated with the holotype specimen, and most are incomplete. The capitulum is rather small and is supported by a long and gently curved neck. The tuberculum is elliptical in shape and forms a shoulder area on the rib. The shaft is long and particularly robust; it curves laterally, tapering to a compressed distal tip. Its cranial surface is convex, whereas its caudal surface is flat. Its medial border is thinner than its lateral border. A prominent ridge curves ventrally from the rostradorsal edge of the tuberculum across the cranial surface of the shaft.

*Sacrum.*—In the holotype specimen, the massive sacral piece is composed of 15 vertebrae. This character was regarded as diagnostic by Godefroit et al. (2003). Unfortunately, this piece is crushed and most centra are completely obscured by the fused ilia (Fig. 16A). Therefore, it is not possible to recognize each vertebra precisely. It is in fact highly probable that true sacral vertebrae are less numerous and that several posterior dorsal vertebrae and, maybe, one or two caudal vertebrae from the proximal region fused with the sacrum. It must be remembered that this specimen was probably an old adult, and that several other bones are fused together. The sacrum is visible in right

lateral view in the referred specimen AEHM 2/846, but the centra are also obscured by the articulated right ilium (Fig. 16B). In this specimen, probably a younger adult, the sacrum is apparently formed of 9 or 10 true sacrals, plus one dorsosacral and one caudosacral, the usual numbers observed in hadrosaurids (Horner et al. 2004). The ventral surfaces of the sacral centra are slightly grooved. The neural spines of the sacrals are slightly higher than those of the adjacent dorsals and caudals (Fig. 15C). In both specimens, the lateral sides of the neural spines of the sacrals are made rigid by a dense double-layered lattice of ossified tendon that extends onto the caudal portion of the dorsals and onto the proximal part of the caudals. In the holotype, the neural spines are completely fused together, whereas they remain well separated in AEHM 2/846.

*Caudal vertebrae.*—The tail of *Olorotitan arharensis* is composed of 70 vertebrae. The complete series was discovered in connection in the holotype specimen. The first vertebra was destroyed during excavation. The centra of the proximal three caudals are slightly procoelous; the others are amphiplatyan (Fig. 17C). In proximal caudal vertebrae, the centra are about two times higher than long (Fig. 17A) and the articular surfaces are sub-rectangular. The centra progressively diminish in size towards the end of the tail. The centra become proportionally longer and less high (Fig. 17B), and the articular surfaces become hexagonal. Caudal ribs are fused to the lateral side of the centra on the proximal 14 vertebrae (Fig. 17C), their size progressively diminishing back through the series. They are dorsoventrally flattened and inclined ventrally and caudally. The lateral sides of the centra are slightly depressed. The ventral side is very concave and forms four large haemaphyseal facets (Fig. 17C); the distal facets are usually better developed than the proximal ones. The neural arch of the caudal vertebrae is less robust than that of the dorsal vertebrae and the size of the medullary canal is smaller. The prezygapophyses are inclined medially, whereas the postzygapophyses are similarly inclined laterally. The pre- and postzygapophyses apparently articulated up to the level of the 50<sup>th</sup> caudal. The size of the zygapophyses and of the medullary canal progressively decreases towards the end of the tail. The neural spine of the proximal caudal vertebrae is high, about twice as high as the centrum and six times as high as long. All are inclined distally. The neural spines are straight in the proximal part of the tail (Fig. 17A), but, from the 17<sup>th</sup> caudal, they become curved (Fig. 17B). They usually have, on their lateral sides, strong longitudinal ridges, marking the insertion of powerful tendons that made the tail rigid. Traces of ossified tendons are observed on the proximal part of the tail up to the 19<sup>th</sup> caudal. The apex of the neural spines is usually roughened and expanded, both proximodistally and transversely. Around the 20<sup>th</sup> caudal, the apices of adjacent neural spines even contacted each other, forming some kind of additional articulation that made this part of the vertebral column particularly rigid: the proximal border of the distal spine forms a knob-like process that inserts into a cup-shaped depression on the distal border of the preceding (Fig. 17D). Of course, this may be a pathological character, or an ontogenetic character relating to

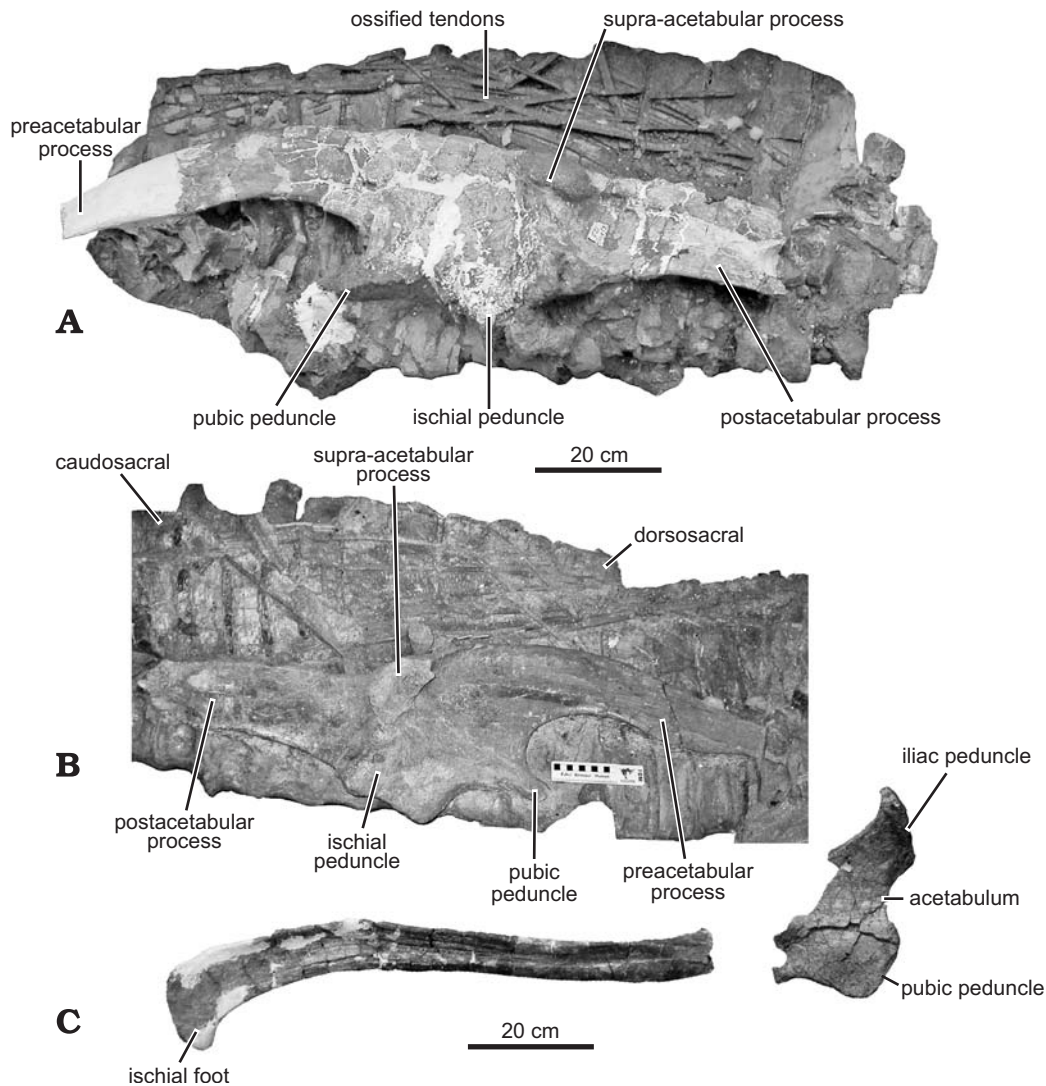


Fig. 16. Hadrosaurid dinosaur *Olorotitan arharensis* Godefroit, Bolotsky, and Alifanov, 2003, from the Upper Cretaceous of Kundur (Russia). **A.** Sacral block and left ilium of AEHM 2/845 (holotype), in lateral view. **B.** Sacrum, caudal part of the dorsal vertebrae and right ilium of AEHM 2/846, in lateral view. **C.** Left ischium of AEHM 2/845 (holotype), in medial view.

the great age of the animal. In any case, there are numerous clear repaired fractures of the neural spines (on Cd 16 and 30, for example). Both the centra and neural arches of the 66<sup>th</sup> and 67<sup>th</sup> caudals are fused together. Only the last two caudals are apparently devoid of a neural arch (Fig. 17E).

**Chevrons.**—Most of the chevrons were found in articulation with the tail of the holotype. Unfortunately, the greatest part was lost during transportation of the specimen from the field to Blagoveschensk. In the proximal part of the tail, the height of the chevrons more or less corresponds to the height of the corresponding neural spines; distally, it is always much lower and more slender. Their caudoventral orientation was also apparently equivalent to the caudodorsal angle of the neural spine.

#### *Pectoral girdle and forelimb*

**Scapula.**—Both scapulae are nearly complete in the holotype (Fig. 18A, B). They are particularly long and slender, reach-

ing about the level of the 10<sup>th</sup> dorsal rib. The L/W ratio of the scapula is about five and was overestimated in Godefroit et al. (2003). The scapular head is less expanded than in *Sahaliyana elunchunorum* (Godefroit et al. 2008: fig. 8a). It is weakly curved in lateral view as in *Corythosaurus casuarius*, *Lambeosaurus lambei*, *Lambeosaurus magnicristatus*, and not as strongly down-turned as in *Parasaurolophus walkeri* (Suzuki et al. 2004; Evans and Reisz 2007). The pseudo-acromion process is laterally directed and located more caudally than in *Sahaliyana elunchunorum* and *Amurosaurus riabinini*. It extends dorsally along the dorsal border of the scapula as a short, but prominent deltoid ridge that extends to the level of the greatest constriction of the scapula (Fig. 18A). The deltoid ridge delimits a wide triangular fossa on the lateral side of the scapula, which may represent the attachment area for *M. supracoracoideus* (Dilkes 2000). The coracoid suture is large and cup-shaped. On the medial side of the scapula, a strong rounded ridge extends from the

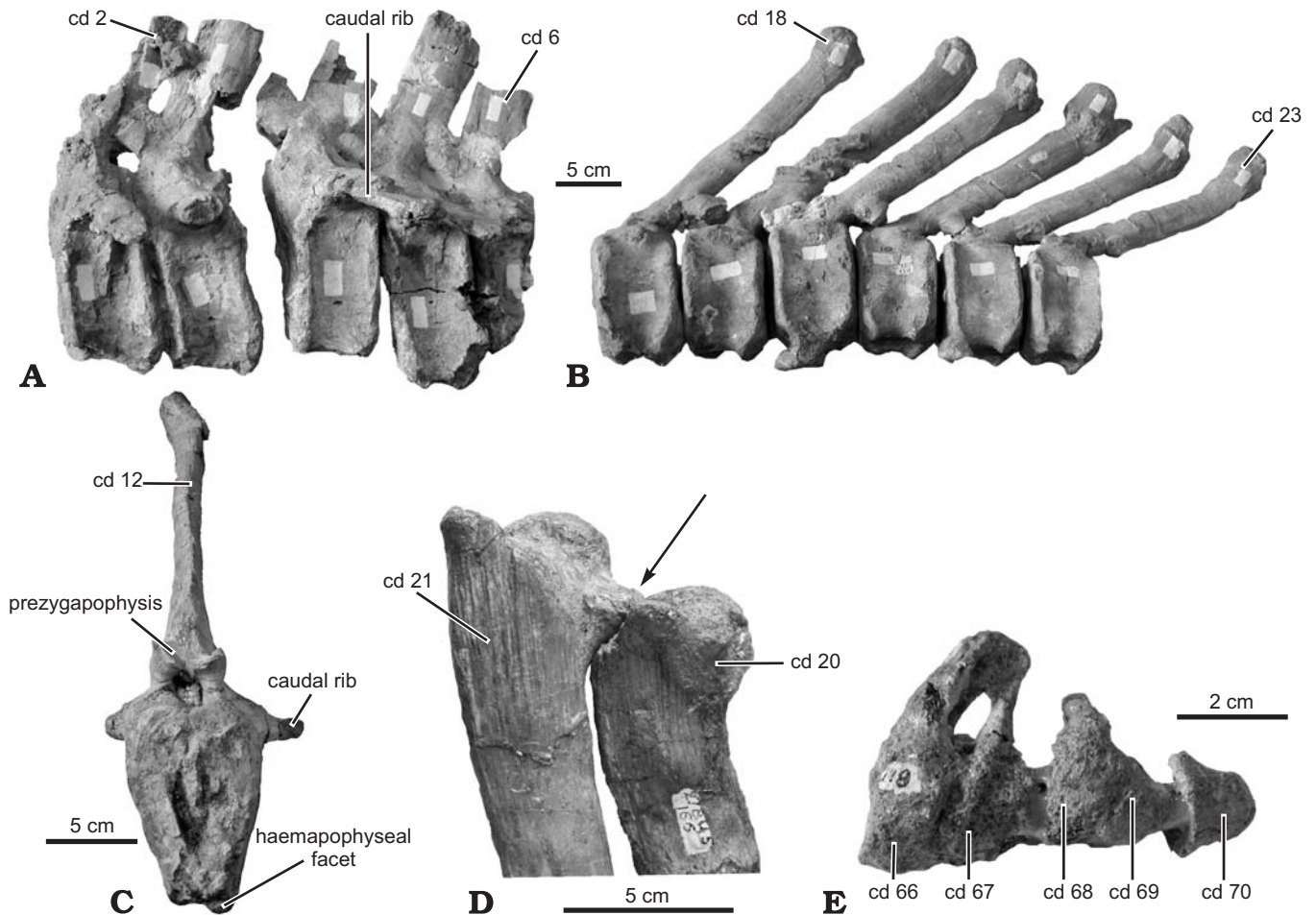


Fig. 17. Caudal vertebrae of hadrosaurid dinosaur *Olorotitan arharensis* Godefroit, Bolotsky, and Alifanov, 2003 (AEHM 2/845, holotype), from the Upper Cretaceous of Kundur (Russia). **A.** Caudal vertebrae 2–6, in left lateral view. **B.** Caudal vertebrae 18–23, in left lateral view. **C.** Caudal vertebra 12, in cranial view. **D.** Supplementary articulation (indicated by an arrow) between the neural arches of caudal vertebrae 20–21. **E.** Caudal vertebrae 66–70, in left lateral view. Abbreviation: cd, caudal vertebra.

coracoid suture to the level of the neck constriction. The glenoid forms a long crescentic depression, subequal in size to the coracoid suture, along the ventral part of the scapular head. It is supported by a prominent caudal buttress that faces slightly laterally. The scapular blade is long, narrow, flat, and particularly thin. It is not curved medially as in *Sahaliyanian elunchunorum* (Godefroit et al. 2008). In lateral view, the neck constriction is long, but not very marked: the minimum constriction at the neck is about 70 percent the maximum height of the blade (53% in *Lambeosaurus magnicristatus*; Evans and Reisz 2007). The ventral and dorsal borders of the scapular blade become straight and perfectly parallel caudal to the neck constriction.

**Coracoid.**—The coracoid closely resembles that of *Amurosaurus riabinini* in being particularly massive (Fig. 18C). The sternal process is prominent and hook-like. Its cranioventral border is rough, indicating the presence of a cartilaginous cap in life. Both the medial and lateral sides of the sternal process are ornamented by radiating ridges suggesting an extensive attachment site for a powerful *M. coracobrachialis*. Dorsal to the sternal process, the lateral side of the coracoid

forms a prominent knob, whose dorsolaterally-facing surface served as attachment site for a strong *M. biceps*. Under the bicipital knob, the coracoid has a well-marked depressed area for insertion of *M. triceps coracoscapularis*. The elliptical coracoid foramen is located in the middle of the bone. On the dorsal part of the coracoid, the articular surface for the scapula is wide and rough, with numerous knobs and depressions. The glenoid forms a wide cup-shaped surface that faces slightly laterally. The articular surface for the scapula and the glenoid form together an angle of about 120°.

**Sternal.**—Both sternals were discovered fused together in the holotype (Fig. 18D). As is usual in Styracosterna, they are typically hatchet-shaped and, as is usual in lambeosaurines, the proximal plate is widened. But, contrary to *Amurosaurus riabinini* (Godefroit et al. 2004b: fig. 13b) and *Sahaliyanian elunchunorum* (Godefroit et al. 2008: fig. 8b), the proximal plate remains shorter than the caudolateral process. Both the proximal and distal borders of the sternal are roughened, indicating the presence of extensive cartilaginous caps. The ventral side of the proximal plate is slightly convex medio-laterally, whereas its dorsal side is slightly concave. The lat-

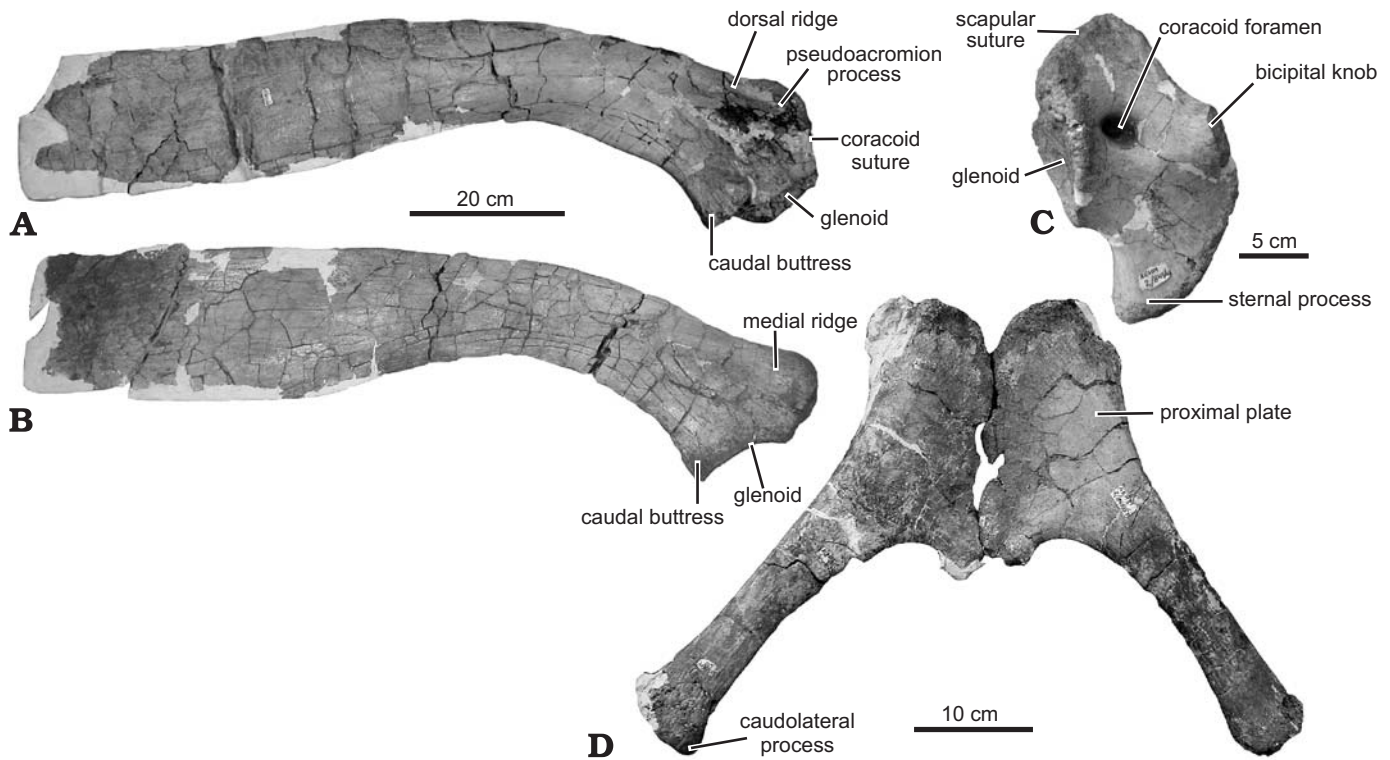


Fig. 18. Hadrosaurid dinosaur *Olorotitan arharensis* Godefroit, Bolotsky, and Alifanov, 2003 (AEHM 2/495, holotype), from the Upper Cretaceous of Kundur (Russia). **A.** Right scapula, in lateral view. **B.** Left scapula, in medial view. **C.** Right coracoid, in lateral view. **D.** Sterna, in ventral view.

eral border of the proximal plate is particularly thin and convex, whereas its proximomedial corner is thickened. The ventral surface of the proximal plate has well marked longitudinal striations around the proximal border of the bone. The caudolateral process of the sternal is straight and massive. Its ventral side is convex mediolaterally, whereas its dorsal side is flat. Its distal end is slightly enlarged. It is not curved dorsally as in *Amurosaurus riabinini* (Godefroit et al. 2004b: fig. 13b) and *Sahaliyania elunchunorum* (Godefroit et al. 2008: fig. 8b). Both sides of the caudolateral process have well-marked longitudinal striations.

**Humerus.**—Only the left humerus is preserved in the holotype. As is usual in lambeosaurines, this bone is particularly massive and the deltopectoral crest is enlarged, extending well below the midpoint of the bone (Fig. 19A). Godefroit et al. (2008: fig. 9) showed that the width of the deltopectoral crest is isometrical to the length of the humerus in lambeosaurines and that the development of the deltopectoral crest in the holotype of *Olorotitan arharensis* fits the general pattern. The lateral border of the deltopectoral crest is regularly convex and only slightly turned cranially (Fig. 19A<sub>3</sub>). Distal to the midshaft, the deltopectoral crest forms a sharp angle to shaft. The proximal articular head forms a rounded buttress on the caudal side of the humerus and is supported by a well-developed rounded crest that extends halfway down the deltopectoral crest (Fig. 19A<sub>2</sub>), as also in *Charonosaurus jiyinensis* (Godefroit et al. 2001). Lateral to the humeral head, a depressed area marks the insertion of *M. triceps humeralis posticus*, as observed in other lambeosaurines

(Godefroit et al. 2001, 2004b). Medial to the humeral head, a less markedly depressed area indicates the insertion of *M. scapulo-humeralis*. Both the inner and outer tuberosities are poorly developed on the proximal part of the humerus. On the cranial side of the bone, the bicipital gutter is less developed than in *Charonosaurus jiyinensis* (Godefroit et al. 2001). The distal portion of the humerus is slightly twisted outwards. The ulnar (medial) condyle is better developed than the radial (lateral) condyle and the olecranon fossa forms a triangular depressed area on the caudal side of the distal humerus (Fig. 19A<sub>2</sub>).

**Ulna.**—Although the right ulna and radius described herein were not found in connection with the humerus (the right humerus is missing), but close to the head of the animal, it is assumed that they belong to the holotype, because of the corresponding size and state of preservation. The ulna is about 5% longer than the humerus. It is proportionally much less elongated and slender than in *Charonosaurus jiyinensis* (Godefroit et al. 2001: pl.6:1). The bone is nearly straight both in cranial and lateral views (Fig. 19B), whereas it is distinctly sigmoidal in *Amurosaurus riabinini* (Godefroit et al. 2004b: fig. 14b). The olecranon process is only poorly developed. The lateral proximal process is virtually absent, but the triangular medial proximal process is high and directed mainly medially and slightly dorsally. Proximally, the cranial surface of the ulna forms a shallow and wide depression against which the proximal part of the radius articulated; longitudinal striations indicate strong ligamentous attachment with the radius. Under this area, the body of the ulna is cranio-

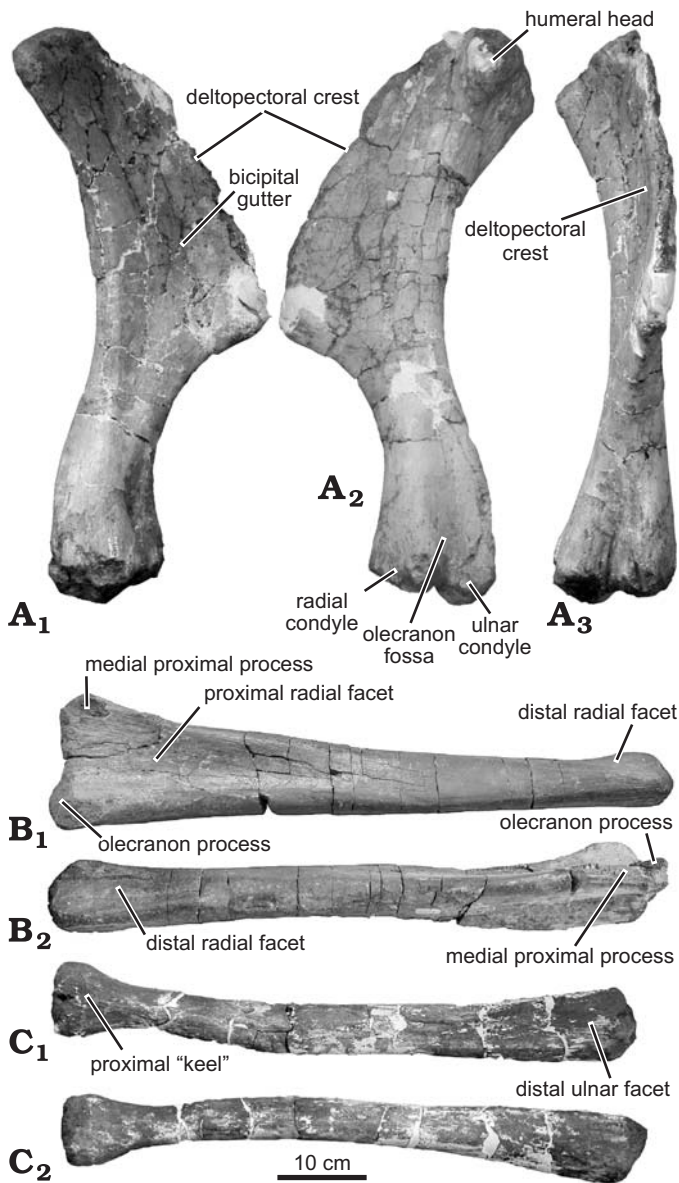


Fig. 19. Hadrosaurid dinosaur *Olorotitan arharensis* Godefroit, Bolotsky, and Alifanov, 2003 (AEHM 2/845, holotype), from the Upper Cretaceous of Kundur (Russia). **A.** Left humerus, in cranial (A<sub>1</sub>), caudal (A<sub>2</sub>), and lateral (A<sub>3</sub>) views. **B.** Right ulna, in cranial (B<sub>1</sub>) and medial (B<sub>2</sub>) views. **C.** Right radius, in caudal (C<sub>1</sub>) and cranial (C<sub>2</sub>) views.

caudally high. It remains triangular in cross section along its whole length. The ulna progressively tapers distally, and the distal end is rounded and laterally compressed. The large triangular articular surface for the distal end of the radius faces craniomedially; it also has strong longitudinal striations, indicating strong ligamentous attachment with the distal part of the radius.

**Radius.**—Like the ulna, the radius is much less elongated than in *Charonosaurus jiyainensis*. It is also nearly perfectly straight (Fig. 19C). The proximal part of the radius is moderately expanded and, as is usual in hadrosaurids, resembles the top of a Doric column in cranial view. Its cranial side is slightly convex, whereas its caudal side is flattened where it

articulated with the proximal part of the ulna. At some distance from the proximal end, the caudal side of the radius forms a strong keel-like prominence (Fig. 19C<sub>1</sub>) that fits into the U-shaped depression on the cranial side of the ulna. Longitudinal striations indicate strong ligamentous attachment of the proximal head of the radius with the ulna. The distal end of the radius is also moderately expanded. Its flattened caudolateral side forms a wide, strongly striated, triangular surface, which fitted against the distal part of the ulna. A strong lateral ridge limits this surface.

#### *Pelvic girdle and hindlimb*

**Ilium.**—Both ilia are incompletely preserved in the holotype (Fig. 16A) and referred specimen AEHM 2/846 (Fig. 15B). The ilium closely resembles that of lambeosaurines usually attributed to the *Corythosaurus* lineage by Brett-Surman (1989), and including *Amurosaurus riabinini* (Godefroit et al. 2004b; fig. 15b) and *Sahaliyana elunchunorum* (Godefroit et al. 2008; fig. 10a). The preacetabular process forms a long and tapering projection from the craniodorsal edge of the iliac blade. It is moderately deflected ventrally (angle of ventral deflection = 154°, see Prieto-Márquez 2010a; character 232) and proportionally very long, as in *Charonosaurus jiyainensis* and *Sahaliyana elunchunorum*: the ratio “ilium length/preacetabular length” is 2.06 in *Olorotitan arharensis* (referred specimen AEHM 2/846) and around 2.1 in *Charonosaurus jiyainensis* and *Sahaliyana elunchunorum* (Godefroit et al. 2001, 2008). Therefore, the great elongation of the preacetabular process can no longer be regarded as an autapomorphy of *Charonosaurus jiyainensis* (contra Godefroit et al. 2000, 2001). The proximal region of the preacetabular process is particularly deep: the ratio between this and the dorsoventral distance between the pubic peduncle and the dorsal margin of the ilium (Prieto-Márquez 2010a; character 233) is 0.66 in AEHM 2/846. The lateral side of the preacetabular process is perfectly flat. Its dorsal edge is thickened and rounded, whereas its ventral edge is sharper. The central blade of the ilium is nearly as high as long. The short supra-acetabular process is much less developed than in *Charonosaurus jiyainensis* (Godefroit et al. 2001; fig. 17), extending lateroventrally less than half the dorsoventral depth of the ilium. Its ventrolateral margin is widely arched, with a slightly caudally skewed profile in lateral view. The pubic peduncle is much shorter than in *Parasaurolophus walkeri* (Parks 1922: pl.6). The iliac portion of the acetabulum is shallow. The ischial peduncle is cranio-caudally elongated. Its articular surface faces caudoventrally and is formed by two sub-rectangular protrusions of similar size separated by a well-marked depression; the caudalmost one is located slightly dorsally (Fig. 16B). A brevis shelf-like structure, at the base of the postacetabular process, is present in the holotype AEHM 2/845 (but apparently absent in the referred specimen AEHM 2/846). Prieto-Márquez (2010a; character 244) also observed such a structure in *Secernosaurus koerni*, *Hypacrosaurus altispinus*, and *Velafrons coahuilensis*. The postacetabular process appears slightly shorter than the central plate and subrectangular in lateral view, with nearly

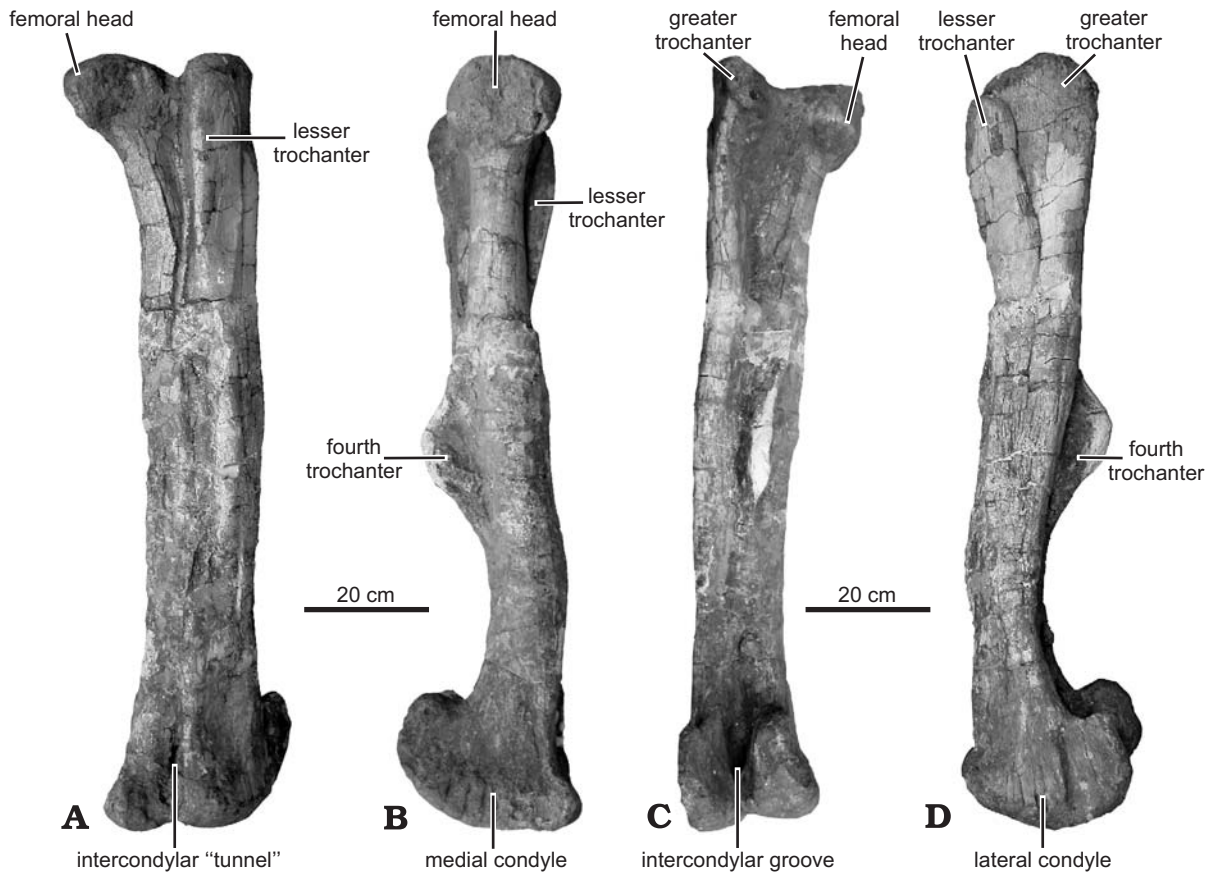


Fig. 20. Left femur of hadrosaurid dinosaur *Olorotitan arharensis* Godefroit, Bolotsky, and Alifanov, 2003 (AEHM 2/845, holotype), from the Upper Cretaceous of Kundur (Russia), in cranial (A), medial (B), caudal (C), and lateral (D) views.

parallel dorsal and ventral borders. In the holotype AEHM 2/845, the dorsal margin of the postacetabular process is nearly parallel with the acetabular margin; it is more caudo-dorsally oriented in AEHM 2/846.

*Ischium*.—Although it is incompletely preserved, the left ischium of the holotype is typical for lambeosaurines: the ischial shaft is long and very robust, gently sigmoidal in lateral view (Fig. 16C). The distal expansion is less prominent than in *Hypacrosaurus altispinus* and *Parasaurolophus cyrtocristatus*. Between its thicker dorsal and its thinner ventral margins, the medial side of the ischial shaft forms a deep sulcus with strong longitudinal striations. The medial side of the ischial foot is also strongly striated, indicating important ligamental attachment between paired ischia. The proximal region of the ischium is well expanded. The iliac peduncle projects cranio-dorsally as a large foot-like process. Its dorsal articular surface is expanded both mediolaterally and dorsoventrally and is elliptical in cross section. The pubic peduncle is more slender and less differentiated than the iliac peduncle. It is cranio-caudally elongated and very compressed mediolaterally. The articular facet for the pubis is subrectangular in cross section and rugose.

*Femur*.—The left femur is preserved in the holotype. In comparison with other lambeosaurines, it appears relatively slender. In caudal view, it is not perfectly straight, but slightly

bowed medially (Fig. 20C), but this could have arisen from post-mortem deformation. The femoral head is robust, but not particularly prominent, and set at an angle to the shaft (Fig. 20A, C). It is better developed craniocaudally than proximodistally (Fig 20B). On the cranial side of the proximal femur, a strong rounded ridge supports the femoral head (Fig. 20A). The lesser trochanter is also prominently developed at the cranio-lateral angle of the proximal femur. It is closely appressed to the greater trochanter, being separated by a deep cleft (Fig. 20D). An extensive flattened and striated area on the lateral side of the lesser trochanter probably marks the insertion area of a powerful *M. ilio-femoralis* (see Norman 1986; Dilkes 2000). Between the lesser trochanter and the cranial crest from the femoral head, the cranial side of the proximal femur forms a deep U-shaped sulcus that might have served as attachment area for a powerful *M. pubo-ischio-femoralis internus 2* (Fig. 20A; see discussion in Norman 1986). The greater trochanter is more extended craniocaudally than the femoral head (Fig. 20D), but its apex lies a little lower than that of the latter (Fig. 20C). The lateral side of the greater trochanter is depressed and scarred by a large triangular insertion area for *M. ilio-trochantericus 1*. The greater trochanter extends as a prominent rounded crest along the caudolateral side of the femur (Fig. 20C). The fourth trochanter forms a prominent, thin, and triangular process along the caudomedial

side of the femur. Its apex lies exactly at mid-height of the bone. Its entire medial side is deeply excavated by a large insertion area for a powerful *M. caudi-femoralis longus* (Fig. 20B). The sulcus between the lateral side of the fourth trochanter and the distal part of the caudal crest of the greater trochanter can be interpreted as the insertion area for *M. caudi-femoralis brevis* (Fig. 20C). The distal condyles are expanded craniocaudally, with regularly convex articular surfaces. The medial condyle is larger than the lateral condyle. The distal condyles are more prominent caudally than cranially (Fig. 20B, D). Cranially, the condyles are fused together to form an intercondylar “tunnel” that surrounded and protected the distal tendon of *M. ilio-tibialis* above the knee (Fig. 20A). Caudally, the distal condyles are separated from each other by a wide and deep flexor intercondylar groove (Fig. 20C). The lateral surface of the lateral condyle has a prominent vertical ridge separating the flattened caudal “heel” region from the more cranial lateral surface of the condyle (Fig. 20D). The whole marginal surface of the distal condyles is rough, with strong vertical striations, indicating the presence of an extensive cartilaginous cap in life.

**Tibia.**—The left tibia, fibula, astragalus and calcaneum are preserved in the holotype, and the four elements are fused distally, indicating that it was an old individual. The tibia is exactly the same length as the femur and, compared with other hadrosaurids, it also appears relatively slender. The cnemial crest is remarkably shorter than in other hadrosaurids, occupying only about the proximal fifth of the tibia (Fig. 21B). It is oriented quite laterally, forming a 90° angle with the tibial shaft. The medial side of the proximal head of the tibia is regularly convex. Its caudal corner forms a large internal condyle separated by a deep, but narrow groove from the smaller lateral condyle. Below the cnemial crest, the tibial shaft is long, straight, and ovoid in cross-section. Proximally, its long axis is oriented craniocaudally, but it progressively becomes oriented mediolaterally toward its distal end (Fig. 21A). The tibial shaft has a prominent lateral ridge that extends distally to form the lateral corner of the external malleolus. The distal end of the tibia is mediolaterally enlarged. The external malleolus is prominent distally. The distal fibula covers its cranial side. Its craniodistal surface articulates both with the calcaneum and the astragalus. The internal malleolus is particularly prominent medially and its distal surface articulates with the astragalus (Fig. 21A).

**Fibula.**—The fibula is slender. Its proximal end is transversely compressed and moderately widened craniocaudally, but it does not really form a cranial peg as usually observed in lambeosaurines such as *Charonosaurus jiyinensis* (Godefroit et al. 2001: fig. 21), and *Amurosaurus riabinini* (Godefroit et al. 2004b: fig. 16). The diameter of the fibula decreases progressively distally and the minimal craniocaudal constriction of the shaft is well below its midpoint (Fig. 21A). Distally, the shaft twists laterally such that the distal third of the fibula lies against the cranio-lateral surface of the tibia. The distal end of the fibula expands cranially into a

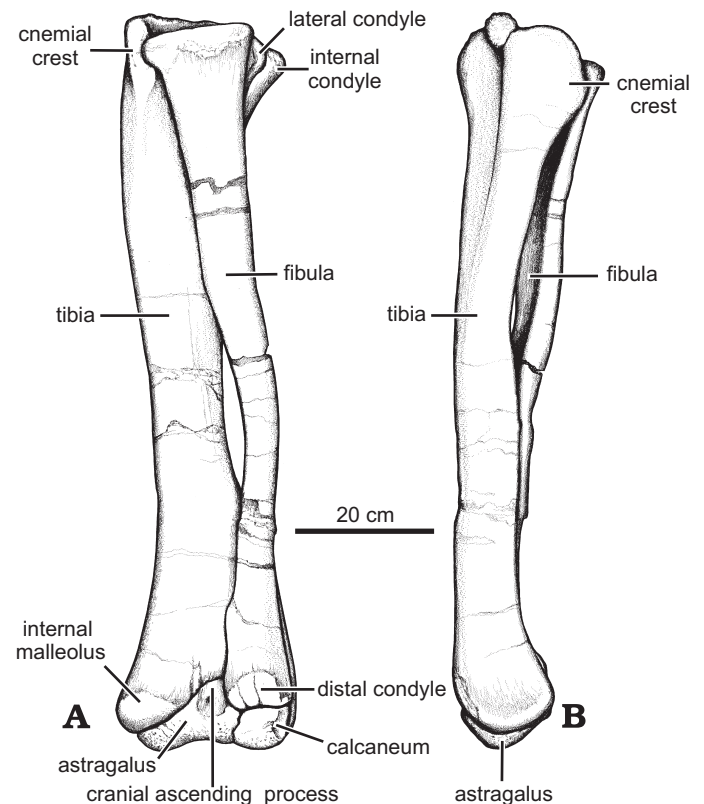


Fig. 21. Left tibia, fibula, astragalus, and calcaneum of hadrosaurid dinosaur *Olorotitan arharensis* Godefroit, Bolotsky, and Alifanov, 2003 (AEHM 2/845, holotype), from the Upper Cretaceous of Kundur (Russia), in cranial (A) and medial (B) views.

rounded, club-shaped condyle (Fig. 21A). The size of this distal expansion is comparable with that of *Corythosaurus casuarius* (ROM 845), *Lambeosaurus lambei* (ROM 1218), *Lambeosaurus magnicristatus* (Evans and Reisz 2007), and *Amurosaurus riabinini* (Godefroit et al. 2004b: fig. 16), but it is less robust than in *Parasaurolophus cyrtocristatus* and *Charonosaurus jiyinensis* (Godefroit et al. 2001). The flattened distal surface of the fibula fits against the dorsal surface of the calcaneum, whereas the medial part of the distal expansion lies against the dorsal surface of the astragalus, lateral to the cranial ascending process (Fig. 21A).

**Astragalus.**—The astragalus is closely appressed to the distal articular surface of the tibia. Laterally, it contacts the calcaneum and its dorsolateral surface fits against the distal expansion of the fibula (Fig. 21A). In ventral view, it appears more elongated mediolaterally and more compressed craniocaudally than in *Amurosaurus riabinini* (Godefroit et al. 2004b: fig. 17a). The triangular caudal ascending process is mediolaterally elongated but low and accommodates against the caudodistal side of the tibia. It is set medially, but unlike in *Charonosaurus jiyinensis*, does not form the cranio-medial angle of the astragalus (Godefroit et al. 2001: fig. 22). The cranial ascending process is higher and set on the cranio-lateral corner (Fig. 21A). In cranial view, the astragalus is sub-triangular and distinctly skewed laterally, as normal in

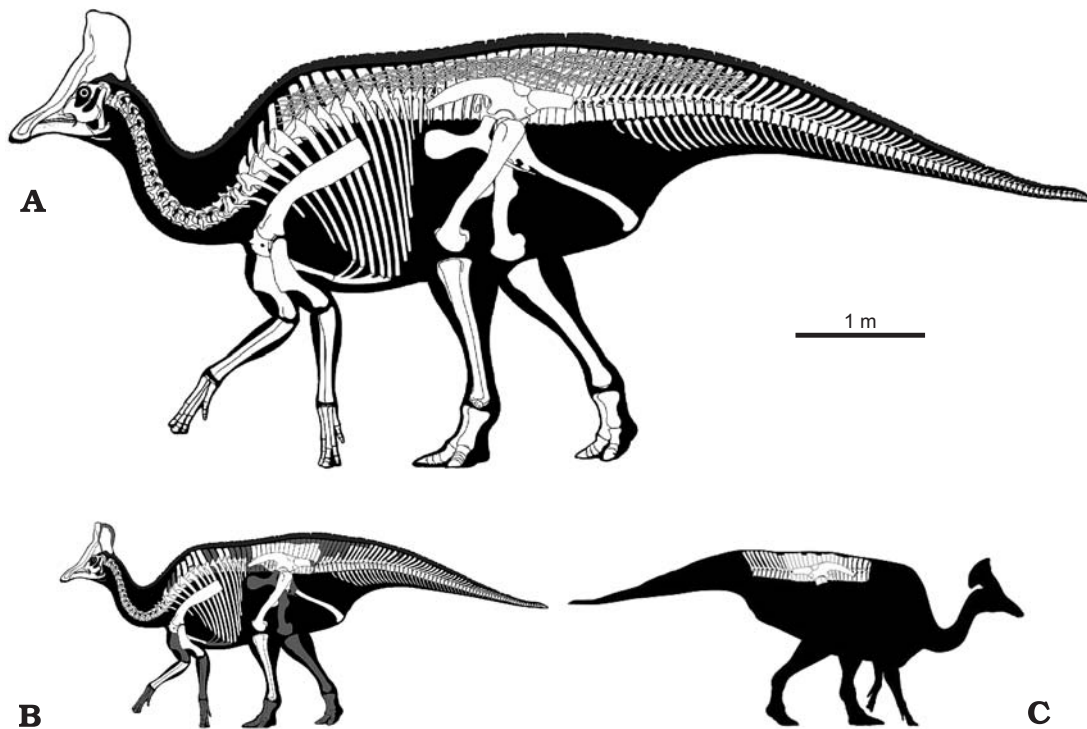


Fig. 22. A. Reconstruction in a quadrupedal gait of the skeleton of hadrosaurid dinosaur *Olorotitan arharensis* Godefroit, Bolotsky, and Alifanov, 2003, from the Upper Cretaceous of Kundur (Russia). B. Preserved bones in holotype AEHM 2/845 (gray). C. Preserved bones in AEHM 2/846.

North American hadrosaurids (Brett-Surman 1989). It is more symmetrical in *Amurosaurus riabinini* (Godefroit et al. 2004b: fig. 17a) and nearly equilateral in *Parasaurolophus cyrtocristatus* (Brett-Surman 1989) and *Charonosaurus jia-yinensis* (Godefroit et al. 2001: fig. 22). As is usual in lambeosaurines, the cranial side of the cranial ascending process is strongly depressed. The roughened ventral side of the astragalus is regularly convex craniocaudally and concave mediolaterally.

**Calcaneum.**—The calcaneum is small and much more elongated craniocaudally than mediolaterally (Fig. 21A). It is confined between the cranial side of the distal tibia, the ventral surface of the distal expansion of the fibula and the lateral side of the astragalus. Its ventral side is roughened and regularly rounded. Its lateral side is subtriangular in shape and shallowly depressed; its dorsal border, which articulates with the distal fibula, is longer than its caudal border that articulates with the tibia.

## Ontogenetic stage, body size, and posture

Many characters concur to suggest that AEHM 2/845 was an old adult individual at the time of its death: fusion of paired sternals, of tibia, fibula, astragalus and calcaneum, of peri-sacral centra, of neural spines of sacrals, of caudal ribs and caudal centra, presence of an additional articulation between ad-

jacent caudal neural spines, and the great amount of repaired fractures. The referred specimen AEHM 2/846 probably belongs to a younger adult: although of equivalent size, the peri-sacral centra are not fused with the sacrum and the sacral neural spines remain well individualized. When mounted in a quadrupedal gait (Fig. 22), AEHM2/845 measures 8 m in length and about 3.5 m in height at the level of the hip. Its femur length is 1.1 m, which corresponds to the average size of the femur in adult hadrosaurids from North America (see Lull and Wright 1942: tables 4–8).

In AEHM 2/845, the tibia is as long as the femur. The tibia is usually slightly shorter than the femur in other hadrosaurids and also in other large Iguanodontia (Table 1). The tibia tends to be longer than the femur in smaller and more cursorial basal ornithopods (see Galton 1974: table 5). The forelimb of *Olorotitan arharensis* and other hadrosaurids is proportionally shorter relative to the hindlimb than in *Iguanodon bernissartensis* (Table 1). Moreover, the forearm is proportionally more elongated relative to the humerus in *Olorotitan arharensis* and in hadrosaurids than in the more basal iguanodontoids *Mantellisaurus atherfieldensis* and *Iguanodon bernissartensis*. The proportions of the forelimb therefore suggest that *Olorotitan arharensis* was primarily bipedal, as also suggested by Galton (1970) for other hadrosaurids. However, trackways made by hadrosaurids indicate that at least some walked both bipedally and quadrupedally and probably were able to change gaits when appropriate (Thulborn 1982; Horner et al. 2004).

Anderson et al. (1985) observed that the mid-shaft cir-

Table 1. Proportions of the limbs in iguanodontoid dinosaurs.

Taxon			femur/tibia	humerus+radius/femur+tibia	radius/humerus
<i>Olorotitan arharensis</i>	AEHM 2/845	Lull and Wright (1942)	1	0.56	0.99
<i>Edmontosaurus regalis</i>	ROM 801		0.807	0.558	0.923
" <i>Anatotitan</i> " <i>copei</i>	AMNH 5730		0.836	0.492	0.806
<i>Gryposaurus incurvimanus</i>	ROM 764		0.903	0.536	0.881
<i>Prosaurolophus maximus</i>	ROM 787		0.865	0.536	0.889
<i>Saurolophus osborni</i>	AMNH 5220		0.887	0.567	1.016
<i>Corythosaurus casuarius</i>	AMNH 5338		0.937	0.582	1.056
<i>Lambeosaurus clavinitialis</i>	CMN 322		0.98	0.562	1.184
<i>Hypacrosaurus altispinus</i>	CMN 8501		0.926	0.546	1.216
<i>Mantellisaurus atherfieldensis</i>	IRSNB R57		Norman (1986)	0.934	0.527
<i>Iguanodon bernissartensis</i>	IRSNB R51	0.88		0.66	0.62

circumferences of the humerus and the femur are closely related to the body weight in living terrestrial vertebrates and proposed two equations for estimating body weight in dinosaurs:  $W = 0.16 C_f^{2.73}$  for bipedal dinosaurs and  $W = 0.078 Ch_{h+f}^{2.73}$  for quadrupedal, where  $C_f$  is the circumference at mid-shaft of the femur and  $Ch_{h+f}$  is the sum of the circumferences at mid-shaft of the humerus and the femur. The estimated weights for AEHM 2/845, the holotype of *Olorotitan arharensis*, are 2635 kg if this hadrosaurid was really primarily bipedal, and 3422 kg if it was primarily quadrupedal; its actual mass likely fell somewhere between these values. These weight estimates fit with those calculated by Anderson et al. (1985: table 4) for *Hypacrosaurus altispinus* (CMN 8501: 2000 kg), *Edmontosaurus regalis* (CMN 2289: 3800 kg) and "*Anatotitan*" *copei* (AMNH 5730: 4000 kg), and by Evans (2010) for *Hypacrosaurus altispinus* (CMN 8501: 2000–3300 kg).

## Phylogenetic analysis

A phylogenetic analysis was conducted to assess the relationships of *Olorotitan arharensis* within Lambeosaurinae, based on the data matrix of Evans and Reisz (2007). Some characters were modified and we added 23 characters from the global analysis of Hadrosauridae by Prieto-Márquez (2010a), which we considered to be informative in the context of the Lambeosaurinae. We also included in this analysis the Spanish taxa *Pararhabdodon isonensis* (sensu Prieto-Márquez and Wagner 2009: including *Koutalisaurus kohlerorum*) and *Arenysaurus ardevoli* (Pereda-Suberbiola et al. 2009). *Velafrons coahuilensis* (Gates et al. 2007) and *Sahaliyana elunchunorum* (Godefroit et al. 2008) were first included in this analysis, but subsequently removed because they were identified as "wildcard" taxa responsible for important instabilities in the phylogenetic analysis (a total polytomy within the corythosaurine clade, see below). *Blasisaurus canudo* (Cruzado-Caballero et al. 2010) was published after completion of the phylogenetic analysis. *Probactrosaurus gobiensis* Rozhdestvensky, 1966, *Bactro-*

*saurus johnsoni* Gilmore, 1933, and *Gryposaurus notabilis* Lambe, 1914 were chosen as successive outgroups.

The 118 characters (character list in Appendix 2 and data matrix in Appendix 3) were equally weighted and analysed with TNT 1.1 (Goloboff et al. 2003). A heuristic search of 10000 replicates using random addition sequences, followed by branch swapping by tree-bisection-reconnection (TBR; holding ten trees per replicate) was conducted. The trees were subsequently analysed using Winclada ver.1.00.08 (Nixon 2002), with fast and slow optimizations. To assess the repeatability of tree topologies, a bootstrap analysis was performed (1000 replicates with the heuristic algorithm in Winclada). Bremer support was assessed by computing decay indices with TNT 1.1.

The maximum parsimony analysis resulted in a single tree of 175 steps (Fig. 23; tree description in Appendix 4). The consistency index (CI) is 0.76 and the retention index (RI) is 0.83. This tree is similar to those previously published by Godefroit et al. (2003, 2004b, 2008), Evans and Reisz (2007), Pereda-Suberbiola et al. (2009), and Evans (2010): a series of Asian (*Aralosaurus tuberiferus*, *Tsintaosaurus spinorhinus*, *Jaxartosaurus aralensis*, and *Amurosaurus riabinini*) and European (*Pararhabdodon isonensis* and *Arenysaurus ardevoli*) taxa form successive outgroups to a larger clade formed by Parasaurolophini (taxa more closely related to *Parasaurolophus walkeri* than to *Corythosaurus casuarius*) and Corythosaurini (taxa more closely related to *C. casuarius* than to *P. walkeri*) (Brett-Surman 1979, Godefroit et al. 2004a; Evans and Reisz 2007). The Asian *Tsintaosaurus spinorhinus* and the European *Pararhabdodon isonensis* are regarded as sister taxa, as previously hypothesized by Prieto-Márquez and Wagner (2009) and Prieto-Márquez (2010a). *Olorotitan arharensis* is placed within Corythosaurini, a quite robust clade in this analysis (bootstrap value of 96%). Indeed, it displays the following unambiguous (that do not change placement under both fast and slow optimizations) apomorphies: the caudolateral process of the premaxilla is elongated above the prefrontal (character 6), the hollow crest is raised into a large vertical fan (character 10), the rostral end of the nasal fits along the ventral edge of the caudodorsal process of the premaxilla (character 17 [1]), the number of cervical vertebrae is greater

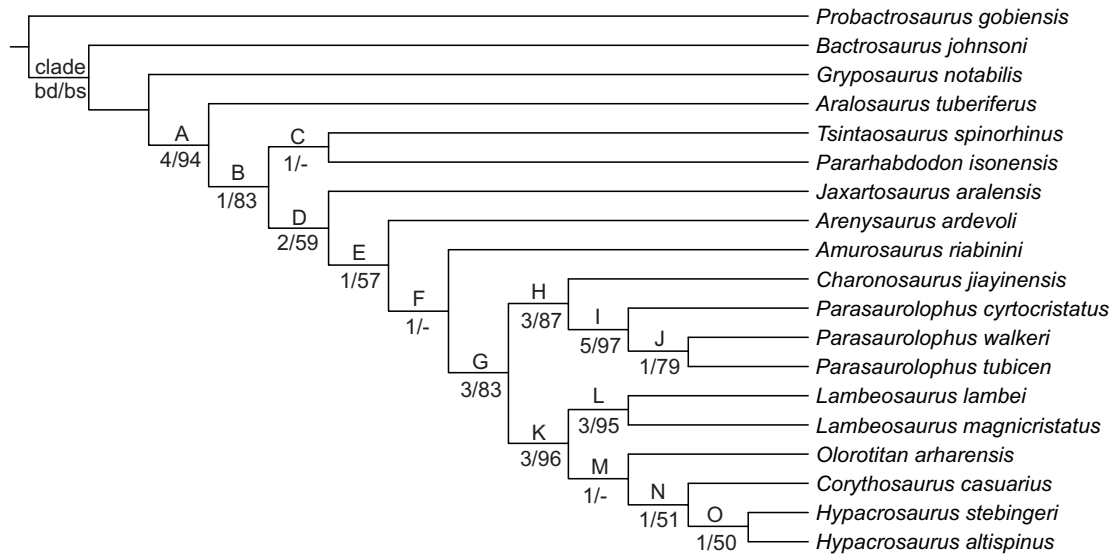


Fig. 23. Most parsimonious tree recovered from the phylogenetic analysis of Lambeosaurinae. Tree length = 175 steps, consistency index (CI) = 0.76; retention index (RI) = 0.83. Character list modified from Evans and Reisz (2007), see Appendix 2 for a list of modified and supplementary characters, Appendix 3 for the data matrix, and Appendix 4 for the tree description.

than 13 (character 66), and the radius is longer than the humerus (character 79). The position of *O. arharensis* within Corythosaurini is more problematic: Bremer and bootstrap values indicate that the phylogenetic relationships between *O. arharensis*, *Corythosaurus casuarius*, *Hypacrosaurus stebingeri*, and *H. altispinus* are particularly weakly supported. These four taxa share the following unambiguous apomorphies: the apex of the helmet-shaped crest is located above the orbits and the nasal forms a large plate-like portion of the caudal external crest surface (character 11), the caudal margin of the of the hollow crest is composed of nasals, which form a long internasal joint along the caudal and caudoventral margin of the crest (character 16 [2]), and the caudoventral region of the nasal is ventrally recurved and hook-shaped, with a rostral process that inserts under the caudolateral process of the premaxilla (character 95). *O. arharensis* is placed as the sister taxon of *Corythosaurus casuarius*, *Hypacrosaurus stebingeri*, and *H. altispinus*, which share the following unambiguous apomorphies: the premaxilla and nasal meet in a complex W-shaped interfingering suture in which a long, finger-like process of the nasal has an extensive overlapping joint with caudodorsal process of the premaxilla in the rostral region of the crest (character 17 [2]) and the caudal region of the caudolateral process of the adult premaxilla is dorsoventrally broad and directed caudally, or caudally and slightly dorsally (character 97 [1], except in *H. altispinus*, which more closely resembles the condition encountered in *Lambeosaurus* ssp.).

The cladogram (Fig. 23) differs from that proposed by Prieto-Márquez (2010a) in the reversed position of the Russian lambeosaurines *Olorotitan arhanrensis* and *Amurosaurus riabinini*. Prieto-Márquez (2010a: fig. 6) hypothesized that *A. riabinini* has closer relationships with *Corythosaurus* ssp., *Lambeosaurus* ssp., and *Hypacrosaurus stebingeri*, and that *O. arharensis* occupies a more basal position in the

cladogram, as the sister taxon of the Corythosaurini + Parasaurolophini clade. He considers that the following two apomorphies are lacking in *O. arharensis*, but are present in all other lambeosaurines except *Tsintaosaurus spinorhinus*, *Pararhabdodon isonensis*, *Jaxartosaurus aralensis*, and *Aralosaurus tuberiferus*: rostral apex of the rostral process of the jugal reduced to a blunt convexity and dorsal margin of the infratemporal fenestra lying below the level of the dorsal margin of the orbit. However, the straight rostral margin of the rostral process of the jugal, as seen in *O. arharensis* (character 28 [2]), is a character shared with *Hypacrosaurus altispinus* (Evans 2010). And the dorsal margin of the infratemporal fenestra is more likely above the dorsal margin of the orbit in *O. arharensis*: the impression that it is located below the dorsal margin of the orbit, on the left side of the braincase in AEHM 2/845, results from post-mortem crushing of the caudal ramus of the postorbital and of the postorbital ramus of the squamosal (Fig. 4B, C). On the contrary, the dorsal margin of the infratemporal fenestra is located below the dorsal margin of the orbit in *Amurosaurus riabinini*, supporting its basal position in the lambeosaurine phylogeny.

## Palaeobiogeographic implications

An Asian origin for lambeosaurines is now generally admitted (Godefroit et al. 2003, 2004a, b; Pereda-Suberbiola et al. 2009; Prieto-Márquez and Wagner 2009; Prieto-Márquez 2010b; Cruzado-Caballero et al. 2010). According to Pereda-Suberbiola et al. (2009), Prieto-Márquez and Wagner (2009), Prieto-Márquez (2010b), and Cruzado-Caballero et al. (2010), the European occurrences of *Pararhabdodon isonensis* and *Arenysaurus ardevoli* may be explained by dispersal events from Asia no later than the early or middle

Campanian. The other significant dinosaurian faunal connections between Asia and Europe during the Late Cretaceous are the presence of the basal hadrosauroids *Telmatosaurus transsylvanicus* and *Tethyshadros insularis* (Dalla Vecchia 2009), of neoceratopsians (Godefroit and Lambert 2007; Lindgren et al. 2007; Ósi et al. 2010) and of dromaeosaurid theropods (Csiki et al. 2010). Interestingly, the basal position of the Iberian lambeosaurines suggests that the connection with Asia was probably interrupted prior to the Maastrichtian (Cruzado-Caballero et al. 2010).

No later than the late Campanian, lambeosaurines occupied western North America, where they underwent extensive cladogenesis, giving rise to the Parasaurolophini and Corythosaurini clades (Prieto-Márquez 2010b). The presence of a “basal” lambeosaurine (*Amurosaurus riabinini*), a representative of the Parasaurolophini clade (*Charonosaurus jiyinensis*), and a representative of the Corythosaurini clade (*Olorotitan arharensis*) in the Maastrichtian of the Amur-Heilongjiang region indicates that independent lambeosaurine lineages dispersed between western North America and eastern Asia at the end of the Cretaceous. Fiorillo (2008) recently demonstrated that the concept of Beringia, an entity encompassing northeastern Asia, northwestern North America and the surmised land connection between the two regions, should be formally extended back in time to the Cretaceous and is rooted in its accretionary rather than its climatic history. Godefroit et al. (2009) showed that the late Maastrichtian Kakanaut dinosaur fauna in Chukotka (northeastern Russia) more closely resembles the Hell Creek fauna of western North America than the synchronous Amur-Heilongjiang fauna. Therefore, the important differences between the late Maastrichtian dinosaur faunas from the Amur-Heilongjiang region (lambeosaurines dominant, ceratopsids absent) and from western North America (ceratopsids dominant, lambeosaurine completely or virtually absent) cannot be simply explained by the opening of the Bering Strait during the Maastrichtian, but probably reflect palaeoecological differences between these areas.

The apparent patchy distribution of hadrosaurid genera in Maastrichtian localities from the Amur-Heilongjiang region is rather surprising. So far, four main dinosaur localities are known along the borders of the Zeya-Bureya Basin. The distances between these localities are not important (see Fig. 1) and the hadrosaurid fossils have been discovered in the same *Wodehouseia spinata*–*Aquilapollenites subtilis* Palynozone, suggesting that these hadrosaurids are roughly synchronous, from a geological point of view. *Charonosaurus jiyinensis* is limited to the Jiayin locality, *Sahaliyania elunchunorum* and *Wulagasaurus dongi* to Wulaga, *Amurosaurus riabinini* and *Kerberosaurus manakini* to Blagoveschensk, *Olorotitan arharensis* and *Kundurosaurus nagornyi* (Godefroit et al. 2012) to the Kundur locality. Ecological factors, which still have to be investigated, therefore probably led to an important habitat partitioning of hadrosaurid faunas in eastern Asia during the Maastrichtian. Similar habitat partitioning has also been observed in North American hadrosaurids (Horner

et al. 2004). Habitat partitioning between species that have a great potential for dispersion suggests that competition for food resources was very important between hadrosaurid populations that lived in the Amur-Heilongjiang region at the end of the Cretaceous. In modern large vertebrates, habitat partitioning usually implies an elaborate social life. It has been postulated that hadrosaurid circumnasal and supra-cranial features may have been used for both visual and vocal communication, and were implied in species recognition, intraspecific combat, ritualised display, courtship display, parent-offspring communication and social ranking. They would have promoted successful mating within species that live close to each other by acting as premating genetic isolating mechanisms (Hopson 1975; Horner et al. 2004).

## Acknowledgements

The authors thank all participants to the field campaigns at Kundur. The illustrations were drafted by Andrey Atuchin (Figs. 3, 15, 21, 22) and Dina Rogatnyh (Figs. 4, 6, 9, 10) (both AEHM). We are also grateful to Valentina Markevich, Evgenia Bugdaeva (both Institute of Biology and Soil Science FEB RAS, Vladivostok, Russia), and Pascaline Lauters (Royal Belgian Institute of Natural Sciences, Brussels, Belgium) for their support and fruitful discussions. David C. Evans (ROM) and Albert Prieto-Márquez (Bayerische Staatssammlung für Paläontologie und Geologie, Munich, Germany) reviewed a first draft of this paper and made many helpful comments that significantly improved the manuscript. This study was realized through the execution of S&T bilateral co-operation agreements on behalf of the Belgian State, Federal Scientific Policy. The excavations and researches at the Kundur locality were also supported by a grant from the National Geographic Society and by a grant from the Russian Foundation for Basic Research (10-05-00151).

## References

- Alifanov, V.R. and Bolotsky, Y.L. 2002. New data about the assemblages of the Upper Cretaceous carnivorous dinosaurs (Theropoda) from the Amur Region. In: G.L. Kirillova (ed.), *Cretaceous Continental Margin of East Asia: Stratigraphy, Sedimentation, and Tectonics*, 25–26. Unesco-IUGS-IGCP, Khabarovsk.
- Alifanov, V.R. and Bolotsky, Y.L. 2010. *Arkharavia heterocoelica* gen. et sp. nov., a new sauropod dinosaur from the Upper Cretaceous of the Far East of Russia. *Paleontologičeskij žurnal* 2010: 76–83.
- Anderson, J.F., Hall-Martin, A., and Russell, D.A. 1985. Long-bone circumference and weight in mammals, birds and dinosaurs. *Journal of Zoology A* 207: 53–61.
- Averianov, A.O., Bolotsky, Y.L., and Godefroit, P. 2002. First multituberculate mammal from Russia. In: G.L. Kirillova (ed.), *Cretaceous Continental Margin of East Asia: Stratigraphy, Sedimentation, and Tectonics*, 27–28. Unesco-IUGS-IGCP, Khabarovsk.
- Bolotsky, Y.L. and Godefroit, P. 2004. A new hadrosaurine dinosaur from the Late Cretaceous of Far Eastern Russia. *Journal of Vertebrate Palaeontology* 24: 354–368.
- Bolotsky, Y.L. and Kurzanov, S. 1991. The hadrosaurs of the Amur Region. In: V. Moiseyenko (ed.), *Geology of the Pacific Ocean Border*, 94–103. Amur KNII, Blagoveschensk.
- Brett-Surman, M.K. 1979. Phylogeny and palaeoecology of hadrosaurian dinosaurs. *Nature* 277: 560–562.
- Brett-Surman, M.K. 1989. *A revision of the Hadrosauridae (Reptilia:*

- Ornithischia*) and Their Evolution During the Campanian and Maas-trichtian. 272 pp. Unpublished Ph.D. thesis, George Washington University, Washington DC.
- Bugdaeva, E.V. and Markevich, V.S. 2001. The problem of extinction at the Cretaceous–Tertiary boundary. In: E.V. Bugdaeva (ed.), *Flora and Dinosaurs at the Cretaceous–Paleogene Boundary of Zeya-Bureya Basin (IGCP project 434)*, 108–112. Dalnauka, Vladivostok.
- Bugdaeva, E.V., Markevich, V.S., Sorokin, A.P., and Bolotsky, Y.L. 2001. Stratigraphy. In: E.V. Bugdaeva (ed.), *Flora and Dinosaurs at the Cretaceous–Paleogene Boundary of Zeya-Bureya Basin (IGCP project 434)*, 21–43. Dalnauka, Vladivostok.
- Clark, J.R., Beerbower, J.R., and Kietzke, K.K. 1967. Oligocene sedimentation, stratigraphy, paleoecology, and paleoclimatology in the Big Badlands of South Dakota. *Fieldiana Geology* 5: 1–158.
- Cope, E.D. 1869. Synopsis of the extinct Batrachia, Reptilia and Aves of North America. *Transactions of the American Philosophical Society* 14: 1–252.
- Cruzado-Caballero, P., Pereda-Suberbiola, X., and Ruiz-Omeñaca, J.I. 2010. *Blasisaurus canudo* gen. et sp. nov., a new lambeosaurine dinosaur (Hadrosauridae) from the latest Cretaceous of Arén (Huesca, Spain). *Canadian Journal of Earth Sciences* 47: 1507–1517.
- Csiki, Z., Vremir, M., Brusatte, S.L., and Norell, M.A. 2010. An aberrant island-dwelling theropod dinosaur from the Late Cretaceous of Romania. *Proceedings of the National Academy of Sciences* 107: 15357–15361.
- Dalla Vecchia, F.M. 2009. *Tethyshadros insularis*, a new hadrosauroid dinosaur (Ornithischia) from the Upper Cretaceous of Italy. *Journal of Vertebrate Paleontology* 29: 1100–1116.
- Danilov, I.G., Bolotsky, Y.L., Averianov, A.O., and Donchenko, I.V. 2002. A new genus of lindholmemydid turtle (Testudines, Testudinoidea) from the Late Cretaceous of the Amur River Region, Russia. *Russian Journal of Herpetology* 9: 155–68.
- Dilkes, D.W. 2000. Appendicular myology of the hadrosaurian dinosaur *Maiasaura peeblesorum* from the Late Cretaceous (Campanian) of Montana. *Transactions of the Royal Society of Edinburgh: Earth Sciences* 90: 87–125.
- Dodson, P. 1975. Taxonomic implications of relative growth in lambeosaurine hadrosaurids. *Systematic Zoology* 24: 37–54.
- Eberth, D.A. and Getty, M.A. 2005. Ceratopsian bonebeds: occurrence, origins, and significance. In: P.J. Currie and E.B. Koppelhus (eds.), *Dinosaur Provincial Park, a Spectacular Ancient Ecosystem Revealed*, 501–506. Indiana University Press, Bloomington.
- Evans, D.C. 2010. Cranial anatomy and systematic of *Hypacrosaurus altispinus*, and a comparative analysis of skull growth in lambeosaurine hadrosaurids (Dinosauria: Ornithischia). *Zoological Journal of the Linnean Society* 159: 398–434.
- Evans, D.C. and Reisz, R.R. 2007. Anatomy and relationships of *Lambeosaurus magnicristatus*, a crested hadrosaurid dinosaur (Ornithischia) from the Dinosaur Park Formation, Alberta. *Journal of Vertebrate Paleontology* 27: 373–393.
- Evans, D.C., Forster, C.A., and Reisz, R.R. 2005. The type specimen of *Tetragonosaurus erectofrons* (Ornithischia: Hadrosauridae) and the identification of juvenile lambeosaurines. In: P.J. Currie and E.B. Koppelhus (eds.), *Dinosaur Provincial Park, a Spectacular Ancient Ecosystem Revealed*, 349–366. Indiana University Press, Bloomington.
- Evans, D.C., Reisz, R.R., and Dupuis, K. 2007. A juvenile *Parasaurolophus* (Ornithischia: Hadrosauridae) braincase from Dinosaur Provincial Park, Alberta, with comments on crest ontogeny in the genus. *Journal of Vertebrate Paleontology* 27: 642–650.
- Fiorillo, A.R. 1988. Taphonomy of the Hazard Homestead Quarry (Ogallala Group), Hitchcock County, Nebraska. *University of Wyoming Contributions to Geology* 26: 57–98.
- Fiorillo, A.R. 1991a. Taphonomy and depositional settings of Careless Creek Quarry (Judith River Formation), Wheatland County, Montana, USA. *Palaogeography, Palaeoclimatology, Palaeoecology* 81: 281–311.
- Fiorillo, A.R. 1991b. Prey bone utilization by predatory dinosaurs. *Palaogeography, Palaeoclimatology, Palaeoecology* 88: 157–166.
- Fiorillo, A.R. 2008. Dinosaurs of Alaska: implications for the Cretaceous origin of Beringia. *The Geological Society of America Special Paper* 442: 313–326.
- Galton, P.M. 1970. The posture of hadrosaurian dinosaurs. *Journal of Paleontology* 44: 464–473.
- Galton, P.M. 1974. The ornithischian dinosaur *Hypsilophodon* from the Wealden of the Isle of Wight. *Bulletin of the British Museum (Natural History), Geology* 25: 1–152.
- Gates, T.A., Sampson, S.D., Delgado de Jesús, C.R., Zanno, L.E., Eberth, D., Hernández-Rivera, R., Aguillón Martínez, M.C., and Kirkland, J.I. 2007. *Velafrons coahuilensis*, a new lambeosaurine hadrosaurid (Dinosauria: Ornithopoda) from the late Campanian Cerro del Pueblo Formation, Coahuila, Mexico. *Journal of Vertebrate Paleontology* 27: 917–930.
- Gilmore, C.W. 1924. On the skull and skeleton of *Hypacrosaurus*, a helmet-crested dinosaur from the Edmonton Cretaceous of Alberta. *Bulletin of the Canada Department of Mines and Geological Survey* 38: 49–64.
- Gilmore, C.W. 1933. On the dinosaurian fauna of the Iren Dabasu Formation. *Bulletin of the American Museum of Natural History* 67: 23–78.
- Gilmore, C.W. 1937. On the detailed skull structure of a crested hadrosaurian dinosaur. *Proceedings of the United States National Museum* 84: 481–491.
- Godefroit, P. and Lambert, O. 2007. A re-appraisal of *Craspedodon lonzeensis* Dollo, 1883 from the Upper Cretaceous of Belgium: the first record of a neoceratopsian dinosaur in Europe? *Bulletin de l'Institut Royal des Sciences Naturelles de Belgique, Sciences de la Terre* 77: 83–93.
- Godefroit, P., Alifanov, V.R., and Bolotsky, Y.L. 2004a. A re-appraisal of *Aralosaurus tuberiferus* (Dinosauria, Hadrosauridae) from the Late Cretaceous of Kazakhstan. *Bulletin de l'Institut royal des Sciences Naturelles de Belgique, Sciences de la Terre* 74 (supplement): 139–154.
- Godefroit, P., Bolotsky, Y.L., and Alifanov, V.R. 2003. A remarkable hollow-crested hadrosaur from Russia: an Asian origin for lambeosaurines. *Comptes Rendus Palevol* 2: 143–151.
- Godefroit, P., Bolotsky, Y.L., and Lauters, P. 2012. A new saurolophine dinosaur from the latest Cretaceous of Far Eastern Russia. *PLoS ONE* 7 (5): e36849. doi:10.1371/journal.pone.0036849.
- Godefroit, P., Bolotsky, Y.L., and Van Itterbeeck, J. 2004b. *Amurosaurus riabinini*, a Late Cretaceous lambeosaurine dinosaur from Far Eastern Russia. *Acta Palaeontologica Polonica* 49: 585–618.
- Godefroit, P., Dong, Z.M., Bultynck, P., Li, H., and Feng, L. 1998. New *Bactrosaurus* (Dinosauria: Hadrosauridae) material from Iren Dabasu (Inner Mongolia, P.R. China). *Bulletin de l'Institut royal des Sciences Naturelles de Belgique, Sciences de la Terre* 68 (Supplement): 3–70.
- Godefroit, P., Golovneva, L., Shchepetov, S., Garcia, G., and Alekseev, P. 2009b. The last polar dinosaurs: high diversity of latest Cretaceous arctic dinosaurs in Russia. *Naturwissenschaften* 96: 495–501.
- Godefroit, P., Hai, S., Yu, T., and Lauters, P. 2008. New hadrosaurid dinosaurs from the uppermost Cretaceous of northeastern China. *Acta Palaeontologica Polonica* 53: 47–74.
- Godefroit, P., Zan, S., and Jin, L. 2000. *Charonosaurus jiyinensis* n.g., n.sp., a lambeosaurine dinosaur from the Late Maastrichtian of north-eastern China. *Comptes rendus de l'Académie des Sciences de Paris, Sciences de la Terre et des Planètes* 330: 875–882.
- Godefroit, P., Zan, S., and Jin, L. 2001. The Maastrichtian (Late Cretaceous) lambeosaurine dinosaur *Charonosaurus jiyinensis* from north-eastern China. *Bulletin de l'Institut royal des Sciences Naturelles de Belgique, Sciences de la Terre* 71: 119–168.
- Goloboff, P.A., Farris, J.S., and Nixon, K. 2003. *TNT: tree analysis using new technologies*. Program and documentation available from the authors and at <http://www.zmuc.dk/public/phylogeny>
- Hopson, J.A. 1975. The evolution of cranial display structures in hadrosaurian dinosaurs. *Paleobiology* 1: 21–43.
- Horner, J.R., Weishampel, D.B., and Forster, C.A. 2004. Hadrosauridae. In: D. B. Weishampel, P. Dodson, and H. Osmólska (eds.), *The Dinosauria, second edition*, 438–463. University of California Press, Berkeley.
- Koster, E.H. 1987. Vertebrate taphonomy applied to the analysis of ancient fluvial systems. In: F.G. Ethridge, R.M. Flores, and M. D. Harvey (eds.), Recent developments in fluvial sedimentology (Contributions from the Third

- International Fluvial Sedimentology Conference). *SEPM Special Publication* 39: 159–168.
- Lambe, L.M. 1917. A new genus and species of crestless hadrosaur from the Edmonton Formation of Alberta. *The Ottawa Naturalist* 31: 65–73.
- Lindgren, J., Currie, P.J., Siverson, M., Rees, J., Cederström, P., and Lindgren, F. 2007. The first neoceratopsian dinosaur remains from Europe. *Palaeontology* 50: 929–937.
- Loope, D.B., Dingus, L., Swisher, C.C.I., and Minjin, C. 1998. Life and death in a late Cretaceous dune field, Nemegt Basin, Mongolia. *Geology* 26: 27–30.
- Loope, D.B., Mason, J.A., and Dingus, L. 1999. Lethal landslides from eolian dunes. *Journal of Geology* 107: 707–713.
- Lull, R.S. and Wright, N.E. 1942. Hadrosaurian dinosaurs of North America. *Geological Society of America Special Papers* 40: 1–242.
- Markevitch, V.S. 1994. Palynological zonation of the continental Cretaceous and early Tertiary of eastern Russia. *Cretaceous Research* 15: 165–177.
- Markevitch, V.S. and Bugdaeva, E.V. 2001. Correlation of the Upper Cretaceous and Palaeogene plant-bearing deposits of the Russian Far East. In: E.V. Bugdaeva (ed.), *Flora and Dinosaurs at the Cretaceous–Palaeogene Boundary of Zeya-Bureya Basin (IGCP project 434)*, 76–96. Dalnauka, Vladivostok.
- Maryańska, T. and Osmólska, H. 1979. Aspects of hadrosaurian cranial anatomy. *Lethaia* 12: 265–273.
- Nichols, D.J. 2002. Palynology and biostratigraphy of the Hell Creek Formation in North Dakota: a microfossil record of plants at the end of Cretaceous time. In: D.J. Nichols (ed.), *The Hell Creek Formation and the Cretaceous–Tertiary Boundary in the Northern Great Plains: An Integrated Continental Record of the End of the Cretaceous*. *Geological Society of America Special Papers* 361: 393–456.
- Nichols, D.J. and Sweet, A.R. 1993. Biostratigraphy of Upper Cretaceous non-marine palynofloras in a north-south transect of the Western Interior Basin. In: W.G.E. Caldwell and E.G. Kauffman (eds.), *Evolution of the Western Interior Basin*. *Geological Association of Canada, Special Paper* 39: 539–584.
- Nichols, D.J. and Johnson, K.R. 2008. *Plants and the K-T Boundary*. 280 pp. Cambridge University Press, Cambridge.
- Nixon, K.C. 2002. *WinClada ver. 1.00.08*. Published by the author, Ithaca, New York.
- Norman, D.B. 1986. On the anatomy of *Iguanodon atherfieldensis* (Ornithischia, Ornithopoda). *Bulletin de l'Institut royal des Sciences naturelles de Belgique, Sciences de la Terre* 56: 281–372.
- Ósi, A., Butler, R.J., and Weishampel, D.B. 2010. A Late Cretaceous ceratopsian dinosaur from Europe with Asian affinities. *Nature* 465: 466–468.
- Ostrom, J.H. 1961. Cranial morphology of the hadrosaurian dinosaurs of North America. *Bulletin of the American Museum of Natural History* 122: 33–186.
- Owen, R. 1842. Report on British fossil reptiles. *Report of the British Association for the Advancement of Sciences* 9: 60–204.
- Parks, W.A. 1922. *Parasaurolophus walkeri*, a new genus and species of crested trachodont dinosaur. *University of Toronto Studies, Geological Series* 13: 1–32.
- Parks, W.A. 1923. *Corythosaurus intermedius*, a new species of trachodont dinosaur. *University of Toronto Studies, Geological Series* 15: 5–57.
- Parks, W.A. 1931. A new genus and two new species of trachodont dinosaurs from the Belly River Formation of Alberta. *University of Toronto Studies, Geological Series* 31: 1–11.
- Pereda-Suberbiola, X., Canudo, J.I., Cruzado-Caballero, P., Barco, J.L., López-Martínez, N., Oms, O., and Ruiz-Omeñaca, J.I. 2009. The last hadrosaurid dinosaurs of Europe: a new lambeosaurine from the uppermost Cretaceous of Arén (Huesca, Spain). *Comptes Rendus Palevol* 8: 559–572.
- Prieto-Márquez, A. 2008. *Phylogeny and Historical Biogeography of Hadrosaurid Dinosaurs*. 936 pp. Unpublished Ph.D. dissertation, Florida State University, Tallahassee, Florida.
- Prieto-Márquez, A. 2010a. Global phylogeny of hadrosauridae (Dinosauria: Ornithopoda) using parsimony and Bayesian methods. *Zoological Journal of the Linnean Society* 159: 135–502.
- Prieto-Márquez, A. 2010b. Global historical biogeography of hadrosaurid dinosaurs. *Zoological Journal of the Linnean Society* 159: 503–525.
- Prieto-Márquez, A. and Wagner, J.A. 2009. *Pararhabdodon isonensis* and *Tsintaosaurus spinorhinus*: a new clade of lambeosaurine hadrosaurids from Eurasia. *Cretaceous Research* 30: 1238–1246.
- Riabinin, A.N. 1930. *Mandschurosaurus amurensis* nov. gen. nov. sp., a hadrosaurian dinosaur from the Upper Cretaceous of Amur River. *Mémoires de la Société paléontologique de Russie* 2: 1–36.
- Rozhdestvensky, A.K. 1966. New iguanodonts from Central Asia. Phylogenetic and taxonomic relationships between late Iguanodontidae and early Hadrosauridae [in Russian]. *Paleontologičeskij žurnal* 1966: 103–116.
- Seeley, H.G. 1887. On the classification of the fossil animals commonly called Dinosauria. *Proceedings of the Royal Society of London* 43: 165–171.
- Sullivan, R.M. and Williamson, T.E. 1999. A new skull of *Parasaurolophus* (Dinosauria: Hadrosauridae) from the Kirkland Formation of New Mexico and a revision of the genus. *New Mexico Museum of Natural History and Science* 15: 1–52.
- Suzuki, D., Weishampel, D.B., and Minoura, N. 2004. *Nipponosaurus sachalinensis* (Dinosauria: Ornithopoda): anatomy and systematic position within Hadrosauridae. *Journal of Vertebrate Paleontology* 24: 145–164.
- Thulborn, R.A. 1982. Speeds and gaits of dinosaurs. *Palaeogeography, Palaeoclimatology, Palaeoecology* 83: 341–366.
- Tumanova, T.A., Bolotsky, Y.L., and Alifanov, V.R. 2004. The first finds of armored dinosaurs in the Upper Cretaceous of Russia (Amur Region). *Paleontologičeskij žurnal* 38: 73–77.
- Van Itterbeeck, J., Bolotsky, Y.L., Bultynck, P., and Godefroit, P. 2005. Stratigraphy, sedimentology and palaeoecology of the dinosaur-bearing Kundur section (Zeya-Bureya Basin, Amur Region, Far Eastern Russia). *Geological Magazine* 142: 735–750.
- Voorhies, M.R. 1969. Taphonomy and population dynamics of an Early Pliocene vertebrate fauna, Knox County, Nebraska. *Contributions to Geology, University of Wyoming Special Paper* 1: 1–69.
- Weishampel, D.B. and Horner, J.R. 1990. Hadrosauridae. In: D.B. Weishampel, P. Dodson, and H. Osmólska (eds.), *The Dinosauria*, 534–561. University of California Press, Berkeley.
- Weishampel, D.B., Norman, D.B., and Grigorescu, D. 1993. *Telmatosaurus transsylvanicus* from the Late Cretaceous of Romania: the most basal hadrosaurid dinosaur. *Palaeontology* 36: 361–385.
- Young, C.C. 1958. The dinosaurian remains of Laiyang, Shantung. *Palaeontologia Sinica, series C* 16: 1–138.

# Appendix 1

Measurements (in mm).

Parietal (right)	length	78
	rostral width	75
	minimal width	40
Frontal (left)	ectocranial length	39
	width	52
Maxilla (right)	length	363
	height (at dorsal process)	181
Jugal (right)	length	221
	height (at level of postorbital process)	220
Predentary	width	222
	length along lateral process	>138
	height of rostral margin	38
Dentary (left)	length	550
	length of dental battery	340
	distance between rostralmost tooth position and caudal margin of the coronoid process	335
	distance between ventral deflection of dentary and caudal margin of the coronoid process	220
	length of diastema	90
	height at coronoid process	200
	height of dentary ramus at mid-length	81
	labiolingual breadth of dentary ramus at mid-length	59
	distance between symphysis and lateral wall of the dentary	133
	distance between ventral margin of dentary ramus and ventral margin of symphysis	42
	Scapula (right)	length
width of proximal head		206
minimal width (neck constriction)		144
maximal width of scapular blade		207
Coracoid (left)	height (from scapular surface to sternal process)	160
	length (from cranial border of scapular surface to tip of sternal process)	160
	maximal width	80
Sternal (right)	length	420
	length of proximal plate	205
	maximal width of proximal plate	155
	width of distal "handle" at mid-length	50

Humerus (left)	length	615
	length of deltopectoral crest	375
	width of the lateral surface of the proximal end	138
	width of deltopectoral crest	182
	minimal width of humeral shaft	87
	width of distal humerus	119
Ulna (right)	circumference at mid-shaft	190
	length	640
	width (mediolateral) of proximal ulna	128
	height (craniocaudal) of proximal ulna	88
	height at mid-length	48
Radius (right)	width of distal ulna	57
	height of distal ulna	70
	length	620
	width (mediolateral) of proximal radius	80
	height (craniocaudal) of proximal radius	57
Ilium (left)	width of distal ulna	80
	height of distal ulna	61
	length	~1080
	length of preacetabular process	~490
Femur (left)	length of postacetabular process	~290
	height at level of supra-acetabular process	250
	height	1100
	width (mediolateral) of proximal part	248
	length (craniocaudal) of proximal part	164
	width of distal part	195
Tibia (left)	length of distal part	285
	circumference (below fourth trochanter)	440
	height	1100
	length (craniocaudal) of proximal tibia	272
	width (mediolateral) of proximal tibia	177
Fibula (left)	length of distal tibia	166
	width of distal tibia	262
	height	1035
	length (craniocaudal) of proximal fibula	170
Astragalus (left)	length of distal fibula	105
	length (craniocaudal)	110
Calcaneum (left)	width (mediolateral)	166
	length (craniocaudal)	97
	width (mediolateral)	65

## Appendix 2

### Character description

Characters 1–94 were culled from Evans and Reisz (2007). Only modified and supplementary characters are described below.

28. Jugal, rostral process shape. Asymmetrical with a pointed process between the maxilla and lacrimal (0); roughly symmetrical and reduced to a short process or regularly convex (1); straight, nearly vertical rostral margin (2).
83. Ilium. Development of the lateroventral projection of the supra-acetabular process of the ilium (Prieto-Márquez 2010a, character 236): forms a longitudinal and continuous “swelling” or reflected border along the dorsal margin of the central plate and the proximal region of the postacetabular process, with a depth of up to 25% the depth of the ilium (0); projected lateroventrally at least 25% (but less than half) the depth of the ilium (1); projects lateroventrally between half and three quarters of the dorsoventral depth of the ilium (2); projects lateroventrally to overlap totally or at least half of the lateral ridge of the caudal prominence of the ischial peduncle (3).
85. Ilium. Ratio between the craniocaudal length of the postacetabular process and the craniocaudal length of the central plate of the ilium (Prieto-Márquez 2010a, character 243): short postacetabular process, ratio up to 0.80 (0); postacetabular process nearly as long as the central plate, ratio greater than 0.80 but less than 1.1 (1); postacetabular process substantially longer than the central plate, ratio of 1.1 or greater (2).
95. Nasal. Caudoventral region of the nasal ventrally recurved and hook-shaped, with a rostral process that inserts under the caudolateral process of the premaxilla (Prieto-Márquez 2010a, character 80): absent (0); present (1).
96. Maxilla. Morphology of the jugal articulation surface (Prieto-Márquez 2010a, character 92): protruding lateral to the caudal third of the maxilla as a mediolaterally compressed finger-like process directed caudolaterally, separated a short distance from the lateral side of the element (0); process consisting of a promontory located dorsal and rostral to the ectopterygoid shelf, bearing a concave and subtriangular, dorsolaterally facing joint surface for the jugal, with a caudolaterally directed corner (1); subtriangular joint surface for the jugal that is more laterally than dorsally facing, with a lateroventrally-directed pointed corner that is located adjacent and slightly dorsal to the proximal end of the lateral ridge of the ectopterygoid shelf (2); dorsally elevated jugal joint (distance between the ventral margin of the jugal joint and ectopterygoid shelf nearly equal to depth of the caudal segment of the maxilla), caudal margin of the joint flush with the caudal margin of the rostradorsal eminence of the lateral side of the maxilla (3).
97. Premaxilla. Morphology of the caudal region of the caudolateral process of the adult premaxilla (Prieto-Márquez 2010a, character 71): mediolaterally compressed and triangular (0); dorsoventrally broad and directed caudally, or caudally and slightly dorsally (1); triangular and dorsoventrally expanded, laterally convex lobe, directed rostradorsally (2).
98. Location of the dorsal margin of the infratemporal fenestra relative to the dorsal margin of the orbit (Prieto-Márquez 2010a, character 192): the dorsal margin of the infratemporal fenestra lies approximately at the same level as the dorsal margin of the orbit, and the caudal region of the skull roof is subhorizontal or slightly sloping rostroventrally relative to the frontal plane (0); the dorsal margin of the infratemporal fenestra is substantially more dorsally located than the dorsal margin of the orbit, and the caudal region of the skull roof is rostroventrally inclined relative to the frontal plane (1); the dorsal margin of the infratemporal fenestra lies slightly or substantially below the level of the dorsal margin of the orbit, and the caudal region (2).
99. Morphology of the dorsal outline of the supratemporal fenestra (Prieto-Márquez 2010a, character 193): subrectangular, with the long axis directed rostrally (0); oval, with the long axis directed rostrrolaterally (1); oval and wider mediolaterally than rostrocaudally (2).
100. Jugal. Relative depth of the caudal and rostral constrictions (in adults) (rostral constriction region located between the rostral and postorbital processes; caudal constriction region located between the postorbital process and the caudoventral flange) (Prieto-Márquez 2010a, character 113): deeper rostral constriction, ratio of the depth of the caudal constriction relative to the rostral of 1 or less (0); deeper caudal constriction, with a ratio greater than 1 and less than 1.35 (1); much deeper caudal constriction, with a ratio greater than 1.35 (2).
101. Prefrontal. Exposure of the prefrontal-nasal contact in lateral and/or dorsal view (Prieto-Márquez 2010a, character 127): contact totally exposed in lateral and/or dorsal view (0); contact visible in lateral view along the caudal and half of the dorsal margin of the prefrontal (1); contact visible in lateral view only along the caudal region of the prefrontal in adults, because of the invasion of the premaxilla along the medial side of the prefrontal (2).
102. Prementary. Ratio between the prementary maximum mediolateral width and the maximum rostrocaudal length along the lateral process (Prieto-Márquez 2010a, character 22): less than 1.2 (0); between 1.2 and 1.75 (1); more than 1.75 (2).
103. Prementary. Ratio between the dorsoventral depth of the prementary rostral face (excluding the median ventral process) and the length of the lateral process (Prieto-Márquez 2010a, character 23): ratio greater than 0.38 (0); ratio of 0.38 or less (1).
104. Prementary. Number of prementary denticles in adult individuals lateral to the median denticle (not included in the count) (Prieto-Márquez 2010a, character 27, modified): maximum of five (0); six or more (1).
105. Dentary. Lingual projection of the symphyseal region of the dentary (measured as a ratio between the labiolingual extension of the symphyseal region and the maximum labiolingual width of the dentary) (Prieto-Márquez 2010a, character 38, modified): ratio up to 1.65 (0); ratio greater than 1.65 and up to 2.85 (1); extremely elongated rostral end of the dentary, ratio greater than 2.85 (2).
106. Dentary. Medial or lateral profile of the dorsal margin of the rostral edentulous region of the dentary for articulation with the prementary (Prieto-Márquez 2010a, character 40, modified): having a well pronounced concavity (0); almost straight to straight, or even displaying a subtle convexity (1).

107. Surangular. Lateral curvature of the caudal process of the surangular (Prieto-Márquez 2010a, character 55): absent, process nearly straight rostrocaudally (0); present, process laterally recurved (1).
108. Coracoid. Angle between the lateral margins of the facet for scapular articulation and the glenoid (Prieto-Márquez 2010a, character 207): angle greater than  $115^\circ$  (0); angle up to  $115^\circ$  (1).
109. Scapula. Development of the deltoid ridge (Prieto-Márquez 2010a, character 218): dorsoventrally narrow convexity limited to the proximal region of the scapula, near the pseudo-acromion process from which it develops, with a poorly demarcated ventral margin (0); dorsoventrally deep and cranio-caudally long, with a well-demarcated ventral margin (1).
110. Sternal. Length of the "handle-like" caudolateral process of the sternal relative to that of the craniomedial plate (excluding the caudoventral process) (Prieto-Márquez 2010a, character 204): caudolateral process slightly shorter or as long as the craniomedial plate (0); caudolateral process longer than the craniomedial plate (1).
111. Ulna. Length of the ulna relative to its dorsoventral thickness (measured at mid-shaft) (Prieto-Márquez 2010a, character 223, modified): ratio length/width less than 10 (0); ratio length/width equal or larger than 10 (1).
112. Ilium. Dorsoventral depth of the central plate of the ilium (expressed as a ratio between this and the distance between the pubic peduncle and the caudodorsal prominence of the ischial peduncle) (Prieto-Márquez 2010a, character 234): ratio of 0.80 or greater (0); ratio less than 0.80 (1).
113. Ilium. Brevis shelf at the base of the postacetabular process of the ilium (Prieto-Márquez 2010a, character 235, modified): present (0); absent (1).
114. Ischium. Length/width proportions of the pubic peduncle of the ischium (Prieto-Márquez 2010a, character 268, modified): approximately as long proximodistally as the distal articular surface is dorsoventrally wide (0); proximodistally shorter than the dorsoventral width of the distal articular surface (1).
115. Ischium. Dorsoventral thickness of the mid-shaft of the ischium (measured as a ratio between this and the length of the entire shaft) (Prieto-Márquez 2010a, character 270, modified): thick shaft, thickness greater than 5% the length of the ischial shaft (0); thin shaft, up to 5% the length of the ischial shaft (1).
116. Ischium. Orientation of the long axis of the distal "foot" relative to the ischial shaft (Prieto-Márquez 2010a, character 274): straight, ventrally directed (0); cranioventrally directed, the inclination starting at the dorsal margin of the "foot" (1).
117. Length/width proportions of metatarsal III (measured as the ratio between its proximodistal length and its mediolateral breadth at midshaft; Prieto-Márquez 2010a, character 270, modified): ratio less than 4.50 (0); elongated, ratio of 4.50 or greater (1).
118. Length/width proportions of pedal phalanx II2 (Prieto-Márquez 2010a, character 270, modified): subsquared, only slightly shorter proximodistally than it is wide mediolaterally long (0); proximodistally shortened, being twice as wide mediolaterally as it is proximodistally 1(1).

# Appendix 3

Data matrix.

*Probactrosaurus gobiensis*

00000 00000 00000 00000 00000 ?0000 000?0 00000 00?0? ????00 0?000 00000 00000 ????00 00000  
000?? ????00 0?000 00000 0?00? 00000 0?000 ?0000 000

*Bactrosaurus johnsoni*

00000 00000 00000 00000 00?01 ?0000 00000 00000 00000 00000 00000 00000 01010 ?0001 10000  
000?? ????00 10000 10110 10000 00000 00010 00000 000

*Gryposaurus notabilis*

11000 00000 00000 00000 10011 01011 00011 00000 00001 00101 01111 11111 01111 00011 00111  
10001 11112 10000 10110 20101 00000 00011 11?11 010

*Aralosaurus tuberiferus*

????? 00000 00??? 0??10 0101? ????? 000?? 00000 000?0 1010? ?00?? ????? ???? ???? ????  
????? ????? ????? ????0 20011 ????? ????? ????? ???

*Tsintaosaurus spinorhinus*

1???? 00000 000?0 00011 01?1? ????? ?101? 10110 00?00 ?0101 ?0010 11111 11111 ???11 10111  
110?? ????1? 10000 10110 3?02? 01012 10000 10?01 001

*Pararhabdodon isonensis*

????? ????? ????? ????0 11?1? ????? ????? ???? ???? ???? ???? 1???? ????? 0??? ???? ?0011 1????  
110?? ????? ????1? ????? 3???? ????? 1??0? ????? ???

*Arenysaurus ardevoli*

????? 01??? ????? ???? ???? ???? ?111? 10111 01?00 1110? 010?0 111?1 111?1 ?01?1 10111  
10??? ????? 1???? 1???? ???? ???? 0???? ????? ???

*Jaxartosaurus aralensis*

????? ?1??? ????? ???? ???? ???? ?1011 10111 00?00 1010? 0?0?? ???? ???? ???? ????  
????? ????? ????? ???? ???? ???? ???? ???? ???? ???

*Amurosaurus riabinini*

11100 ?1000 001?? 1??11 01?11 ?1111 01111 00111 00110 10111 01010 11111 11111 ?0011 11111  
110?? ????11 1000? 10?1? 20011 ?00?1 01100 10?11 0?1

*Charonosaurus jiayinensis*

????? ?1??? ????? ????11 01?11 ?1111 01??? 01111 02100 11111 01??0 11111 11111 ?0?11 11111  
110?? ????110 1??10 11?10 ????11 ????? 0?10? 101?1 1??

*Parasaurolophus cyrtocristatus*

??110 ?1010 0040? 000?? ????? 1?1?? ?1111 ????12 ????10 1111? 011?0 ????11 111?? ?0111 11111  
11101 ?1110 10111 11??0 ?021? 2???? 0??? ?1101 10?

*Parasaurolophus walkeri*

11110 01010 0140? 00011 01011 11?11 01111 1?112 ????10 11111 ?1110 11011 11111 00111 11111  
11101 11110 101?? 1???0 20212 211?1 0111? ?1111 1??

*Parasaurolophus tubicen*

??11? 01010 0140? 00011 01?11 11111 01111 11112 12110 11111 011?0 11011 11111 ????? ????  
????? ????? ????? ????0 20212 2???? 01??? 0??? ???

*Lambeosaurus lambei*

11111 11101 00311 11111 01?11 11111 01111 00111 01110 11111 11110 11111 11111 10111 11111  
11011 11111 11010 10110 22211 1010? 01101 10011 000

*Lambeosaurus magnicristatus*

1111? 11?01 00311 11111 01111 11111 0111? 00111 01?10 11111 11110 11111 ????11 1???1 111?1  
11011 11111 10010 10??0 22211 1?10? 0??01 10111 00?

*Corythosaurus casuarius*

11111 11101 10211 22011 01111 11111 01111 00111 01110 11111 01110 11111 11111 10111 11111  
11011 11111 11010 10111 21211 20111 01101 10111 001

*Olorotitan arharensis*

11110 11?01 1010? 21011 01?11 11211 0111? 00111 01?10 11111 01?10 11111 111?1 10111 11111  
1101? ????11 ????1? 10??1 20211 ????11 0?101 1001? 0??

*Hypacrosaurus stebingeri*

11111 11101 10102 22011 01111 11111 01111 00111 01110 11111 01110 11111 11111 11111 1?111  
11011 11111 1101? 10111 21211 20110 01101 10101 011

*Hypacrosaurus altispinus*

11111 11101 10102 22111 01111 11211 11110 00111 01110 11111 01110 11111 11111 11111 11111  
11011 11111 11011 10111 22211 2?111 0?101 100?1 011

## Appendix 4

### Tree description

Character transformations were evaluated under unambiguous, fast (ACCTRAN), and slow (DELTRAN) optimisation options in Winclada (Nixon, 2002); unambiguous synapomorphies are those that diagnose a node under both fast and slow optimisations. Node numbers refer to Fig. 22. For simple 0–1 state changes only the character number is given; for other state changes the type of change is specified between brackets.

- Node A (*Lambeosaurinae*): Unambiguous: 19, 22, 46, 99; ACCTRAN: 3, 26, 28, 61, 77, 104, 105, 109(0), 118.
- Node B: Unambiguous: 32, 36, 28, 39; ACCTRAN: 20, 43; DELTRAN: 61, 71, 85, 118.
- Node C: Unambiguous: 96(3), 105(2), 106; ACCTRAN: 99(2), 102, 114(0); DELTRAN: 77.
- Node D: Unambiguous: 7, 40; ACCTRAN: 13, 15, 16, 52, 68, 101(2), 107, 108.
- Node E: Unambiguous: 33; ACCTRAN: 42, 47; DELTRAN: 52, 105.
- Node F: Unambiguous: 36(0), 44, 49, 72; DELTRAN: 3, 13, 20, 28, 43, 77, 107, 108, 114.
- Node G: Unambiguous: 4, 53, 89, 98(2), 103; ACCTRAN: 110; DELTRAN: 26, 47, 68, 101(2).
- Node H (*Parasaurolophini*): 37, 42(2), 85(0), 92, 116; ACCTRAN: 9, 13(4), 16(0), 88, 102; DELTRAN: 113.
- Node I (*Parasaurolophus*): Unambiguous: 40(2), 78, 109, 111(0), 112; ACCTRAN: 36, 41, 58(0), 90, 100(2); DELTRAN: 9, 13(4), 88.
- Node J: Unambiguous: 12; DELTRAN: 36, 58(0), 100(2).
- Node K (*Corythosaurini*): Unambiguous: 6, 8, 10, 17, 23, 66, 79; ACCTRAN: 5, 87; DELTRAN: 15, 42, 110.
- Node L (*Lambeosaurus*): Unambiguous: 13(3), 14, 18, 51, 97(2), 101; ACCTRAN: 104(0), 118(0); DELTRAN: 16.
- Node M: Unambiguous: 11, 16(2), 95; DELTRAN: 104.
- Node N: Unambiguous: 17(2), 97; DELTRAN: 5, 87.
- Node O (*Hypacrosaurus*): Unambiguous: 15(2), 67, 117; ACCTRAN: 90, 114(0).